

**UNIVERSIDAD AUTONOMA DE MADRID**

**ESCUELA POLITECNICA SUPERIOR**



**Grado en Ingeniería de Tecnologías y Servicios de  
Telecomunicación**

## **TRABAJO FIN DE GRADO**

**CARACTERIZACIÓN DE LAS CONDICIONES  
EXPERIMENTALES DE TEST USADAS PARA LA  
EVALUACIÓN DE INTERACCIONES ENTRE CAMPOS  
ELECTROMAGNÉTICOS DE RADIOFRECUENCIA E  
IMPLANTES MÉDICOS EN IMAGEN POR RESONANCIA  
MAGNÉTICA**

**Jose Luis Olivera Cardo**

**Tutor: Juan Córcoles Ortega**

**Ponente: Jorge Alfonso Ruiz Cruz**

**MAYO 2015**



**UNIVERSIDAD AUTONOMA DE MADRID**

**ESCUELA POLITECNICA SUPERIOR**



**Grado en Ingeniería de Tecnologías y Servicios de  
Telecomunicación**

## **FINAL DEGREE WORK**

**CHARACTERIZATION OF EXPERIMENTAL TEST  
CONDITIONS USED FOR THE EVALUATION OF  
INTERACTIONS BETWEEN RADIOFREQUENCY  
ELECTROMAGNETIC FIELDS AND MEDICAL  
IMPLANT DURING MAGNETIC RESONANCE**

**Jose Luis Olivera Cardo**

**Tutor: Juan Córcoles Ortega**

**Ponente: Jorge Alfonso Ruiz Cruz**

**MAY 2015**



## Resumen

La imagen por resonancia magnética (MRI, por sus siglas en inglés) es una de las técnicas que más ha incrementado su popularidad en los últimos años dada su habilidad para obtener imágenes de cierta calidad mediante un proceso no invasivo. Los sistemas MRI emiten pulsos de radiofrecuencia y recogen la respuesta a dicho pulso generada por la muestra sometida a escáner para construir una imagen.

Al realizarse un escáner por resonancia magnética el cuerpo humano se ve sometido a un campo electromagnético de radiofrecuencia. El campo magnético utilizado para la generación de la imagen lleva acoplado un campo eléctrico cuya interacción con los implantes que algunas personas llevan instalados puede llegar a ser peligrosa.

Para evaluar los implantes en términos de seguridad se llevan a cabo los procedimientos indicados en el standard ISO/TS 10974. Una forma de reducir costes, tanto económicos como temporales, es la utilización de software comercial para realizar simulaciones de determinadas pruebas.

El principal problema que plantea el standard ISO/TS 10974 actual es que las posibles trayectorias ofrecidas como ejemplo son demasiado cortas como para situar un implante real a lo largo de las mismas y obtener las condiciones de test deseadas. Por este motivo se han llevado a cabo simulaciones de varias configuraciones de dieléctricos en forma de *phantoms* dentro de un resonador, en donde se han buscado líneas isoeléctricas de unas longitudes mayores, y por lo tanto más cercanas a la de un implante comercial, en línea con lo que actualmente se está haciendo en la revisión del standard. Para poder llegar a estas simulaciones ha sido necesario llevar a cabo un estudio del resonador de radiofrecuencia, encargado de generar el campo electromagnético necesario en el interior de la máquina.

## Abstract

Magnetic resonance imaging (MRI) has experienced a notable growth during the last years because of its ability to produce high quality images without invading the patient's body. MRI systems emit radio frequency pulses and use the signal that the sample returns as a response to the irradiation to build up the image.

When a patient undergoes a magnetic resonance examination, his body is exposed to a radio frequency (RF) magnetic field. The interaction between the electric field that is part of the electromagnetic field and the implants installed in some patients can lead to harmful situations.

With the objective of evaluating, in safety terms, the quality of the implants, the procedures indicated in the technical specification ISO/TS 10974 are carried out. The usage of commercial software to perform certain tests may conduct to substantial money and time savings.

The main drawback presented by the standard ISO/TS 10974 is that the pathways offered as examples are not long enough for commercial implants to be placed and perform the tests in the desired conditions. That is why in this work several phantom-coil configurations were simulated with the objective of finding longer isoelectric pathways where implants can be disposed and successfully tested. Before carrying out the simulations it is convenient to study the functions and design process of the birdcage coil, the device in charge of generating the field required inside the radio frequency coil.

## Palabras Clave/Keywords

### Español

Imagen por resonancia magnética (MRI), relación señal a ruido (SNR), espín, tasa específica de absorción (SAR), precesión, phantom, dispositivo médico implantable (AIMD), inductancia, pulso de radiofrecuencia, bobina de radiofrecuencia, línea isoelectrica, sonda, trayectoria.

### Inglés

Magnetic resonance imaging (MRI), signal-to-noise ratio (SNR), spin, specific Absorption Rate(SAR), precession, phantom, active implantable medical device (AIMD), Inductance, radio frequency (RF) pulse, radio frequency (RF) coil, isoelectric line, lead, pathway.

## Glossary

**MRI:** magnetic resonance imaging is a medical, non-invasive technique used for determining physical structure

**SNR:** Signal-to-noise ratio, a quantity used to compare the power of the signal to the power of the background noise.

**Spin:** fixed-value intrinsic angular momentum possessed by a proton.

**Precession:** movement that takes place when the rotational axis of a rotating object changes its orientation.

**SAR:** specific absorption rate, measure of power dissipated in a biological object.

**Phantom:** object used to simulate biological tissues.

**AIMD:** active implantable medical device, which is intended to be totally or partially introduced, surgically or medically, into the human body, and which, is intended to remain after the procedure

**Inductance:** is the property of a conductor by which a current flowing along it induces a voltage in both the conductor itself (self-inductance) and in any nearby conductors (mutual inductance).

**RF Pulse:** radio frequency oscillation of a determined duration.

**RF Coil:** device that generates the RF pulse inside the magnetic resonance scanner.

**Birdcage:** cage-like RF Coil.

**Isoelectric line:** line that has a relatively uniform ( $\pm 1$ dB of maximum module deviation and 20 degrees of maximum phase deviation) tangent electric field.

**Lead:** flexible tube enclosing one or more insulated electrical conductors, intended to transfer electrical energy along its length.

**Pathway:** line at which an implant lead is disposed.

# Contents

1. Introduction.....	1
1.1. Motivation .....	1
1.2. Goals .....	2
1.3. Structure.....	2
2. Magnetic Resonance Imaging.....	4
2.1. Brief history of Magnetic Resonance Imaging.....	4
2.2. Principles of Magnetic Resonance Imaging.....	4
3. SAR and MRI safety .....	10
3.1. SAR overview.....	10
3.2. IEEE SCC 34 Benchmark, Dipole and Spherical Bowl: Example of SAR computation in SEMCAD X .....	11
3.3. Technical Specification ISO/TS 10974.....	14
3.4. Motivation for updating the standard.....	18
4. Radio-frequency coils .....	20
4.1. Radio-frequency coil description .....	20
4.2. Radio-frequency coil design .....	23
4.2.1. Concept of resonance.....	23
4.2.2. Equivalent circuit analysis.....	26
4.2.3. Calculation of ER Capacitors.....	28
4.2.4. Calculation of Leg Capacitors.....	29
4.3. Example of High-Pass coil construction .....	30
5. Technical Specification ISO/TS 10974 Simulations .....	35
5.1. Phantoms dimensions.....	35
5.2. High Conductivity Medium.....	36
5.3. Low Conductivity Medium .....	41
6. Conclusions .....	45

6.1. Conclusions.....	45
6.2. Future Work.....	46
7. References.....	47
ANNEX I: Dielectric parameters .....	I
ANNEX II: Worst-case phase weighting factors for a single conductive lead ..	II

## List of figures

Figure 2.2.1: Proton-field alignment .....	5
Figure 2.2.2: Precession Movement .....	6
Figure 2.2.3: Longitudinal Magnetization .....	7
Figure 2.2.4: Transversal Magnetization .....	8
Figure 3.2.1: Dipole and spherical bowl .....	12
Figure 3.2.2: Voxel set .....	12
Figure 3.4.1: E-field induced in the phantom along the implant (0dB=71 V/ $\mu$ T) .....	19
Figure 3.4.2: AIMDs examples from Medtronic .....	19
Figure 4.1.1: Circular polarization axial ratio (AR) .....	22
Figure 4.1.2: Branch-line hybrid connected to a coil .....	22
Figure 4.2.1: Birdcage coils .....	23
Figure 4.2.1.1: RLC circuit .....	24
Figure 4.2.2.1: High-pass coil model in SEMCAD X and consecutive legs representation .....	26
Figure 4.2.2.2: Equivalent Circuit .....	28
Figure 4.3.1: Dependence between resonant frequency and capacitance .....	31
Figure 4.3.2: $B_1^+$ for C=66.35 pF .....	32
Figure 4.3.3: $B_1^+$ for C=62.64 pF .....	32
Figure 4.3.4: $B_1^+/B_1^-$ for C=66.35 pF .....	33
Figure 4.3.5: $B_1^+/B_1^-$ for C=62.64 pF .....	33
Figure 4.3.6: Axial ratio for C=66.35 pF .....	34
Figure 4.3.7: Axial ratio for C=62.64 pF .....	34

## List of tables

Table 3.3.1: Incident field value .....	15
Table 3.3.2: High and Low conductivity mediums characteristics .....	15
Table 3.3.3: Incident field constraints .....	18
Table 5.1.1: Phantoms dimensions .....	35
Table 5.2.1: HCM ASTM F2182-11a field plots .....	37
Table 5.2.2: HCM ASTM F2182-11a module and phase along the pathway ..	37
Table 5.2.3: HCM Oval phantom field plots .....	38
Table 5.2.4: HCM Oval phantom module and phase along the pathway .....	39
Table 5.2.5: HCM Circular phantom field plots .....	40
Table 5.2.6: HCM Circular phantom module and phase along the pathway ..	41
Table 5.3.1: LCM Phantoms field plots .....	42
Table 5.3.2: LCM ASTM F2182-11a module and phase along the pathway ..	43
Table 5.3.3: LCM Oval phantom module and phase along the pathway .....	43
Table 5.3.4: LCM Circular phantom module and phase along the pathway ..	44
Table I: Dielectric parameters of body tissue .....	I
Table II: Worst-case phase weighting factors for a single conductive lead (not including helical structures and structures with lumped elements) .....	II

# 1. Introduction

## 1.1. Motivation

Magnetic resonance imaging (MRI) has established itself as one of the most powerful non-invasive imaging techniques. This technology has been playing and will continue to play a leading role in the medical field.

During the MRI process the human body is exposed to a radio-frequency (RF) magnetic field. This exposure implies the interaction between the patient's body and the electric field coupled to the magnetic field (Electromagnetic field). This interaction can be especially dangerous when the person subjected to the scan has a medical implant installed, leading to serious injuries like problems derived from device malfunction or burns produced by the significant increase of the temperature in the surrounding tissues caused by the induced currents along the surface of the implant.

In order to measure the interaction between the electric field and the implant several test and measures are carried out, taking into account some factors such as resonant frequency, field polarization, electromagnetic medium characterization or implant length. Consequently, with the objective of determining whether an implant is considered safe or not the ISO certified the standard ISO/TS 10974 [1], which details the set of test conditions needed to evaluate an implant.

Fortunately, the development of electromagnetic software such as SEMCAD X ([www.speag.com](http://www.speag.com)) or CST Microwave Studio ([www.cst.com](http://www.cst.com)) permits us to reproduce the test conditions, facilitating the study and characterization of the situation before accomplishing an experimental analysis.

## 1.2. Goals

The main goal of this work is the characterization of the set of test conditions needed to demonstrate if an implant is safe when installed inside a patient who undergoes a magnetic resonance examination. The understanding of these conditions will accelerate the assessment, and deliver substantial time and money savings derived from the use of advanced electromagnetic software.

In order to achieve the goals explained in the previous paragraph, a simplified model of an MRI machine was developed, subsequently some phantom-coil configurations were simulated using the commercial software SEMCAD X. Afterwards, data was processed and plotted with the objective of finding the longest possible isoelectric line where implants can be disposed and tested properly [2].

## 1.3. Structure

This work is divided in four parts:

- The first part comprises an introduction to MRI concepts, where the principles of working of that technique are explained.
- The next section is about MRI safety. In this chapter, the concept of SAR (Specific Absorption Rate), which measures the power dissipated in a biological object, is explained. In addition, the key ideas of the current standard [1], which needs to be updated because the implant examples provided are shorter than the ones used in practice, are exposed.
- Before carrying out the simulations of an MRI system it is convenient to study the main element of the scanner, the RF coil. This device is in

charge of generating the pulses that make the imaging process possible.

- Once the RF coil and its purpose were understood, several simulations of phantom-coil configuration were launched. In this simulations we can observe several examples of pathways that are long enough to test commercial implants.

## 2. Magnetic Resonance Imaging

### 2.1. Brief history of Magnetic Resonance Imaging

MRI has experienced an unstoppable development in the second half of the twentieth century, surpassing other imaging techniques. Its importance lies in its ability to produce clear images with remarkable tissue discrimination in any desired plane without radiating the patient.

Felix Bloch and Edward Purcell, both of whom were awarded Nobel Prize in 1952 for their research, discovered magnetic resonance phenomenon in 1946. During the following years nuclear magnetic resonance (NMR) was developed and used as a powerful tool in molecular analysis. Some years later, in 1973 Paul Lauterbur and Peter Mansfield, 2003 Nobel Prize winners, developed a method based on NMR for determining physical structure. Since then MRI has been extensively used in chemical, biomedical and engineering applications.

### 2.2. Principles of Magnetic Resonance Imaging

To understand what happens when a patient is placed in a MR machine is necessary to know the physics behind the MR phenomenon.

Is a well-known fact that atoms consist on a nucleus, comprised of protons and neutrons, and a shell made up of orbiting electrons. Protons in the nucleus are not fully static in their natural state, since they move around a rotation axis just like a planet does. That's to say, a proton possesses an intrinsic angular momentum or spin [3-5].

Naturally the positive charge attached to the proton spins with it, becoming a flow of electrical charge, generating an electric current. As a consequence a magnetic field is induced and a proton can be seen as a small bar magnet which has its own magnetic field.

When put in an external magnetic field ( $B_0$ ) protons align themselves in the direction of the field. There are two possible orientations (parallel or anti-parallel to the field as seen in the following picture) for the proton to point depending on its energy level.

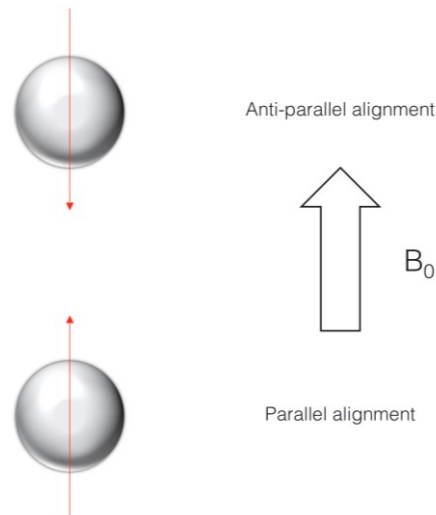


*Figure 2.2.1: Proton-field alignment*

Obviously, the preferred state of alignment is the one that requires less amount of energy, so more protons will align parallel to the field. However, the difference between the number of protons aligned in one direction and the amount of protons aligned in the opposite direction is not significant. For instance for every 10,000,000 protons aligned in the anti-parallel direction there are 10,000,007 aligned parallel to the field [3].

Moreover protons move around in another way, precession movement along the magnetic field lines. During precession the axis of spin performs a circular movement around precession axis as shown in the image below.

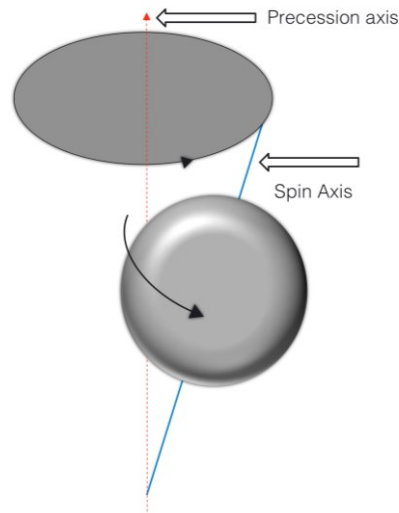


Figure 2.2.2: Precession Movement

In order to obtain useful results during the MRI process is necessary to know how many times the protons precess per second, this magnitude is known as precession frequency. Precession frequency, also known as Larmor frequency, is closely related to the strength of the external magnetic field and can be obtained using the following equation (Larmor equation) where  $B_o$  is magnetic field intensity given in Tesla and  $\gamma$  is the gyro-magnetic ratio given in Megahertz/Tesla.

$$\omega_o [MHz] = B_o [T] \cdot \gamma \left[ \frac{MHz}{T} \right] \quad (2.2.1)$$

Gyro-magnetic ratio is a constant which value is different for each material (for protons  $\gamma = 42.5 \text{ MHz/T}$ ).

From here on protons will be depicted as vectors whose magnitude represents the protons magnetic force.

The next figure shows an example of precession movement along the lines of an external magnetic field parallel to the z-axis. There are five protons aligned parallel to the magnetic field, while only three precess in the other state.

Due to the high speed at which protons move (applying Larmor equation, 64 millions of precessions take place in a second for  $B_0=1.5T$ ), at a certain moment there may be one proton pointing in one direction, and another one pointing in the opposite direction, both of them cancelling their magnetic force. As there are more protons aligned parallel to the external field, some of them do not have their magnetic effects cancelled. Those remaining protons will cancel their magnetic force in the perpendicular directions (x and y) to the magnetic field, and add their effects in the z-axis direction, resulting on a net force pointing parallel to  $B_0$  (red vector in the figure).

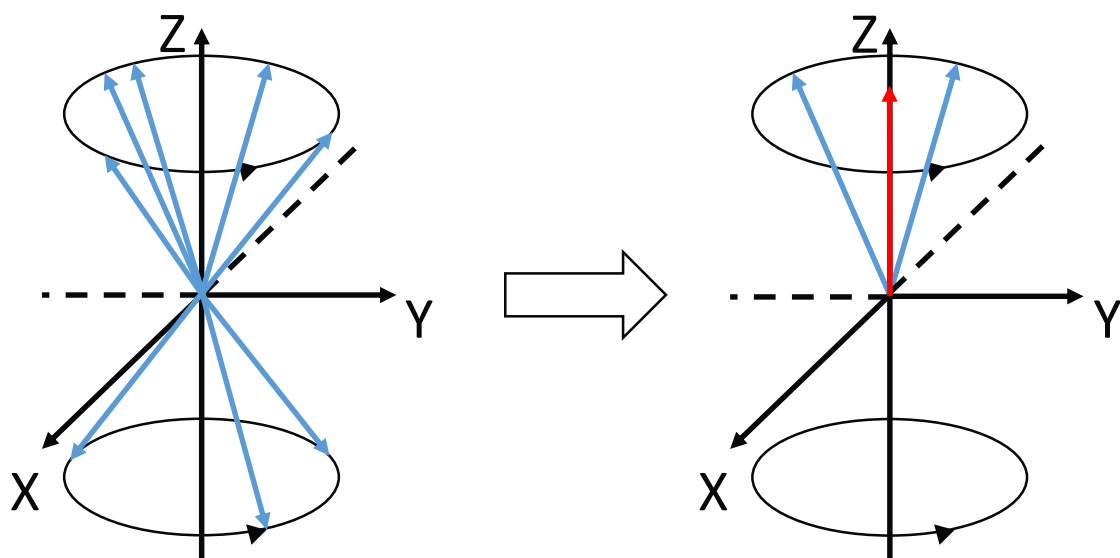


*Figure 2.2.3: Longitudinal Magnetization*

This reasoning leads to the conclusion that a patient placed in an MRI scan behaves as a magnet producing a magneto-static field parallel to the induced field  $B_0$ . This force longitudinal to the magnetic field is called longitudinal magnetization.

With the purpose of building the signal, longitudinal magnetization should be measured, but this is not possible since it is perfectly aligned with the external field and its not feasible to distinguish one from another.

In order to measure the strength of the longitudinal magnetization a radio frequency pulse (short burst of electromagnetic waves) is sent. The pulse disturbs the protons that spin around the precession axis producing a misalignment between  $B_0$  and the longitudinal magnetization vector. To make the energy exchange possible and, therefore, misalign the vectors, the pulse needs to oscillate at the Larmor frequency. This phenomenon is called resonance.

The energy transferred to the protons may change the direction in which they align. As a consequence the longitudinal magnetization will decrease, that is to say, the RF pulse transfers energy from the longitudinal magnetization to the transversal magnetization. Apart from varying the direction of precession the pulse has the ability to synch the protons and make them spin in phase. Transversal magnetization vector is visible and quantifiable.

Transversal magnetization vector moves in line with the precessing protons at Larmor frequency. The next picture shows protons moving in phase and both the transversal and longitudinal magnetization (red arrows).

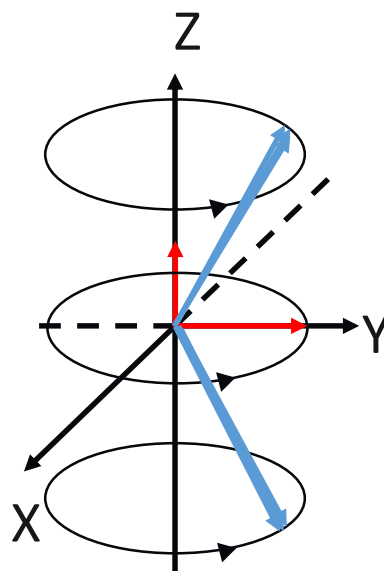


Figure 2.2.4: Transversal Magnetization

As said at the beginning of this section, protons are electric charges, and the movement of electric charges produces electric current. Protons precessing

in phase generate electric current in the receiver probe. The signal received, which concentrates its components around the Larmor frequency, is used to build up the image.

In the last stage of the process, it is possible to determine the origin of the signal by filtering. Several fields of different strength can be used along the patient's body; consequently, each region of interest will generate signals of different frequencies.

### 3. SAR and MRI safety

#### 3.1. SAR overview

As it was discussed before, in order to measure magnetization, protons are excited by a magnetic RF field, often referred as the  $B_1$  field. When the static magnetic field  $B_0$  used has low intensity (lower than 0.5T), Larmor frequency, and consequently  $B_1$  frequency is very small. In this case, the dimension of the patient's body is only a small fraction of the wavelength and the interaction between the body and the field can be ignored. Due to the low SNR achieved in low frequency [6], this systems are not used in practice. With the purpose of improving the quality of the signal, systems with higher intensity  $B_0$  fields have been developed. The usage of higher stronger fields provokes a linear increase in the frequency, hence, ignoring the interaction between the patient and  $B_1$  is not feasible. When this situation occurs, not only the homogeneity of the RF field is significantly degraded, decreasing the quality of the image, but also the patient can be harmed. The increase of temperature caused by the increase of the SAR (Specific Absorption Ratio, measure of power dissipated in a biological object) can damage especially sensitive parts of the body such as the brain and eyes.

$$SAR[W/Kg] = \frac{\text{total RF energy dissipated in sample [J]}}{\text{exposure time [s]} * \text{sample weight [Kg]}} \quad (3.1.1)$$

The power loss  $L$  produced by the conduction current  $\sigma E$  within the lossy volume  $R$  can be calculated as follows:

$$L(R) = \frac{1}{2} \int_R \sigma |E|^2 dv, \quad (3.1.2)$$

where  $|E|^2$  is the squared magnitude of the electric field and  $\sigma$  is the electric conductivity of the sample.

At a given location SAR can be calculated as the ratio between the dissipated power and the mass densities and it can be shown to be proportional to an increase in temperature over time [7-8]:

$$SAR(r) = \frac{\sigma|E|^2}{2\rho} \propto \frac{dT}{dt}, \quad (3.1.3)$$

Where  $\rho$  is the density of the sample and  $T$  is the temperature.

Obtaining local SAR is not always productive, since computational methods approximations introduce notable errors. For this reason SAR is often given in an average form:

- Volume-averaged SAR, used in the MRI scope:

$$\langle SAR \rangle_V = \frac{1}{V} \int_{R(V)} SAR(r) dv \quad [W/m^3] \quad (3.1.4)$$

- Mass-averaged SAR, mainly used in dosimetry studies:

$$\langle SAR \rangle_M = \frac{1}{2M} \int_{R(M)} SAR(r) dm \quad [W/kg] \quad (3.1.5)$$

### 3.2. IEEE SCC 34 Benchmark, Dipole and Spherical Bowl: Example of SAR computation in SEMCAD X

In February 1997 the Standard Coordination Committee 34 (SCC 34) was created (IEEE TC (Technical Committee) 34 at the present time). This committee comprises two subcommittees:

- Subcommittee 1, Experimental techniques: has the purpose of specifying the protocol for the measurement of the average SAR in simplified models of parts of the human body when interacting with RF fields

- Subcommittee 2, Computational techniques: specification of numerical techniques and standardized anatomical models used for computing the SAR. SAR is extracted from the field conditions simulated using Finite Difference Time Domain (FDTD).

Using SEMCAD X the model shown in *Figure 3.2.1* was constructed. This model consists of a bowl, filled with tissue-simulating liquid, irradiated by a dipole placed at a distance of 10 cm. A simulation using a FDTD solver as specified by IEEE SC 34 was carried out.

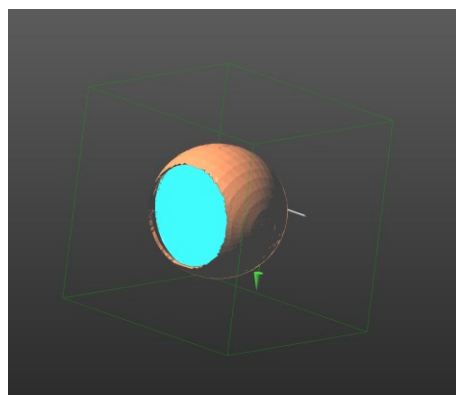


*Figure 3.2.1 Dipole and spherical bowl*

Once the simulation had finished the results were extracted by using a script in python that applies equations 3.1.4 and 3.1.5. The computational equivalent of equations 3.1.4 and 3.1.5 is the sum of the local SAR in the volume of interest. Since three-dimensional models in SEMCAD X are made up of voxels (Volumetric pixels, *Figure 3.2.2*), it was necessary to compute the field inside each voxel.

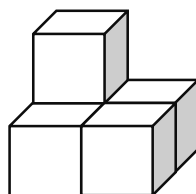


*Figure 3.2.2: voxel set*

The easiest way of doing so was extracting the electric field from  $\vec{D} = \epsilon\vec{E}$ , as the electric induction field  $\vec{D}$  is directly calculated by the software inside each

voxel, whereas the electric field  $\vec{E}$  is computed for all the 4 corners of each voxel, thus requiring interpolation.

Applying the script over the model depicted in the *Figure 3.2.1*, the following averaged SARs were obtained (mass-averaged SAR was checked by using the tool included in SEMCAD X):

$$\langle SAR \rangle_M = 0.469911 [mW/kg]$$

$$\langle SAR \rangle_V = 0.042963 [mW/m^3]$$

### 3.3. Technical Specification ISO/TS 10974

The objective of this technical specification is to establish a set of test conditions in order to evaluate the safety of MRI for patients with AIMD (active implantable medical devices). These specifications are valid for patients having an MRI exam in 1.5T (Larmor frequency: 64 MHz) whole body cylindrical scanner.

Requirements for non-implantable parts as well as requirements for particular AIMDs are not covered by this standard.

The three main hazards related to RF fields are listed below:

- RF field-induced heating of the AIMD: induced currents may cause temperature on the tissues surrounding the leads of the AIMD to rise.
- RF field-induced rectified lead voltage: rectification of induced voltages takes place if the induced voltage is high enough to cause the conduction of non-linear elements (e.g. protection diodes). Rectification can produce voltage pulses on the lead.
- RF field-induced device malfunction: as performance issues are highly dependent on device specifications, they are not extensively described in this standard.

#### **Protection from harm to the patient caused by RF-induced heating**

Measuring temperature increase in tissues due to induced currents is a difficult process, since it depends on several factors such as AIMD design, MRI scanner technology (RF coil and pulse sequence design), patient size, anatomy, position, AIMD location and tissue properties. Elongated metallic devices like pacemakers or neurostimulators leads are more prone to suffer from RF heating.

In order to evaluate the suitability of an AIMD a four-tier approach, in which every tier is more accurate than the previous one, has been developed. Tier 1 offers the simplest accomplishment, whereas Tier 4 requires the strictest EM analysis.

## TIER 1

Step 1: Get from the following table the appropriate incident field depending on the body part and operating mode (RMS stands for root mean square).

<b>Body part</b>	<b>Maximum induced field normalized to B1</b>	<b>Normal mode (2W/kg whole-body SAR)</b>	<b>First level mode (4W/kg whole-body SAR)</b>
		ERMSmax, in vivo	ERMSmax, in vivo
<b>Head</b>	90 V/m/uT	420 V/m	420 V/m
<b>Trunk</b>	140 V/m/uT	500 V/m	700 V/m
<b>Extremities</b>	170 V/m/uT	600 V/m	850 V/m

*Table 3.3.1: Incident field value*

Step 2: Immerse the AIMD in a homogeneous simulated tissue medium (phantoms, which are objects designed to emulate human body's electromagnetic features, are used for this purpose) and expose to a uniform (magnitude and phase) electric test field at the amplitude equal to the value determined in Step 1. If linearity is demonstrated, the test can be carried out with higher or lower field intensities applying the corresponding scaling. Moreover, the results can be scaled up if SNR is higher than 10 dB.

<b>Tissue simulating medium</b>	<b>Relative permittivity</b>	<b>Conductivity (S/m)</b>
<b>High conductivity (HCM)</b>	78	0.47
<b>Low conductivity (LCM)</b>	11.5	0.045

*Table 3.3.2: High and Low conductivity mediums characteristics*

Step 3: Determine the energy deposition from SAR measurements using:

- Numerical assessment with thermal validation
- Numerical assessment with SAR validation
- Full 3D SAR measurements
- Full 3D  $\Delta T$  measurements

Step 4: if the AIMD can be immersed at a depth of 100 mm in the chosen medium, Step 2 and 3 need to be repeated with the remaining medium.

Step 5: the worst-case energy deposition measured in Step 3 shall be multiplied with the corresponding weighting factor. These factors depend on the actual-length/resonant-length (highest energy deposition length) ratio. Weighting factors are shown on Table II from Annex II.

Step 6: the uncertainty level should be fixed in this step according to the requirements showed in annex R.2 of the standard.

Step 7: in vivo temperature rise estimation.

## **TIER 2**

Step 1: EM simulation is required in order to identify the electric and magnetic field magnitudes that will be used during the test. Determine the incident field averaged over 10g of tissue. The following characteristics determine the strength of the field.

- RF frequency
- Body habitus or external anatomy
- Internal anatomy
- Location of the implant
- Transmitting RF coil design and polarization;
- Position in the birdcage with respect to the isocentre
- Body posture in the coil

Step 2 to Step 7: Same steps as in tier 1.

### **TIER 3**

Step 1: Apply Step 1 of tier 2. For structures with a length-to-diameter ratio greater than 10 determine as well the magnetic field averaged over any 20 mm of anatomically relevant elongated AIMD path.

Step 2 to Step 4: Perform Step 2 to Step 4 of Tier 1 using constant phase electric field.

Step 5: Conduct Step 5 of Tier 1. The weighting factor shall be determined as follows:

Option 1: Use the worst-case phase multiplication factor as provided in Table II.

Option 2: find the factor experimentally.

Option 3: Starting with a numerical model of the AIMD, calculate the factor experimentally or numerically by applying an uniform magnitude field with variable phase (phase varies over the range determined in step 1)

Step 6 and Step 7: same as Steps 6 and 7 of Tier 1.

### **TIER 4**

Step 1: Develop and validate an electromagnetic model (full-wave or lumped element) of the AIMD that is being evaluated. The equivalence of the model and experimental results should be proved.

Step 2: Compute the energy deposition normalized to the appropriate incident field, e.g. B1RMS, normal mode, using the validated numerical AIMD model for the defined patient population.

Step 3: Determine the uncertainty of the evaluation.

Step 4: Compute the maximum tissue temperature rise for the energy deposition determined.

## Generation of incident fields for Tier 1 to Tier 3 and minimal medium requirements

Since the generation of incident fields is one of the targets of this work several examples are described in Chapter 5. The test field must meet the following specifications:

<b>Larmor frequency</b>	<b>64 MHz <math>\pm</math> 5 %</b>
<b>B1RMS</b>	<b>&gt; 2 <math>\mu</math>T</b>
<b>Deviation from Uniform Etan-field over the entire AIMD path</b>	<b>&lt; <math>\pm</math> 1 dB (Phase &lt; <math>\pm</math> 20 degrees)</b>

Table 3.3.3: Incident field constraints

For tiers 1, 2 and 3, the phase deviation from uniform Etan-field should be smaller than  $\pm 10$  degrees during the evaluation of maximum amplitude of local energy deposition.

### 3.4. Motivation for updating the standard

The examples provided by the standard described in 3.3 don't correspond to reality, as actual implants are considerably longer than the ones represented in the standard. The following image, extracted from annex M of the standard [1] shows the electric field distribution tangential to the AIMD (parallel to z-axis). The isoelectric condition ( $\pm 1$ dB) is only achieved 314 mm along the line.

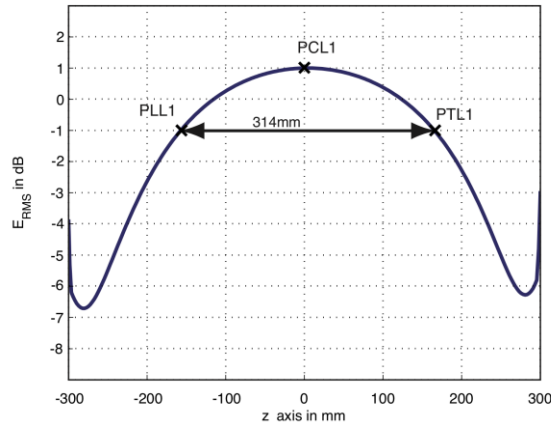


Figure 3.4.1: E-field induced in the phantom along the implant ( $0\text{dB}=71\text{ V}/\mu\text{T}$ )

Examining real pacemakers and spinal chord stimulators leads dimensions from datasheets from brands such as Boston Scientific, Medtronic or Sorin Group we note that their length surpasses considerably the length of 314 mm used as example in the standard. Therefore, an updated version of the standard is being developed [2] with the purpose of offering examples in where actual size AIMDs are used. As the reader may note in the following chapters this work will focus on the configurations that will be included the updated standard.

 <p><a href="#">View larger</a></p>	<p><b>1x8 Vectris SureScan MRI Percutaneous Leads</b> Subcompact Model 977A1 Compact Model 977A2</p>	<ul style="list-style-type: none"> <li>• LENGTH : 60, 75, 90 cm (23.6, 29.6, 35.4 in)</li> <li>• DIAMETER : 1.3 mm (0.05 in)</li> <li>• ELECTRODES : 8</li> <li>• SPACING : Subcompact, compact</li> <li>•  <a href="#">Vectris 1x8 Subcompact and Compact Lead Kit Implant Manual</a></li> </ul>
 <p><a href="#">View larger</a></p>	<p><b>1x8 Percutaneous Leads</b> 1x8 Compact Model 3778 1x8 Standard Model 3777 1x8 Sub-Compact Model 3776</p>	<ul style="list-style-type: none"> <li>• LENGTH : 45, 60, and 75 cm (17.7, 23.6, and 29.5 in)</li> <li>• DIAMETER : 1.3 mm (0.05 in)</li> <li>• ELECTRODES : 8</li> <li>• SPACING : Subcompact, compact, standard</li> <li>•  <a href="#">1x8 Standard, Compact and Sub-Compact Lead Kit Implant Manual</a></li> </ul>
 <p><a href="#">View larger</a></p>	<p><b>1x4 Percutaneous Leads</b> Pisces™ Quad Model 3487A Pisces Quad Compact Model 3887 Pisces Quad Plus Model 3888</p>	<ul style="list-style-type: none"> <li>• LENGTH : 33, 45, and 56 cm (13.0, 17.7, and 22.1 in)</li> <li>• DIAMETER : 1.3 mm (0.05 in)</li> <li>• ELECTRODES : 4</li> <li>• SPACING : Standard, compact, plus</li> <li>•  <a href="#">1x4 Standard, Pisces Quad Leads Implant Manual</a></li> </ul>
 <p><a href="#">View larger</a></p>	<p><b>8-Electrode Surgical Leads</b> Specify Model 3998 Specify 2x4 Hinged Model 3999</p>	<ul style="list-style-type: none"> <li>• LENGTH (Model 3998) : 20 cm (8.27 in)</li> <li>• LENGTH (Model 3999) : 30, 45, and 60 cm (11.8, 17.7, and 23.6 in)</li> <li>• DIAMETER : 1.3 mm (0.05 in)</li> <li>• PADDLE SHAPE, PROFILE : Rectangle, hinged</li> <li>• ELECTRODES : 8</li> <li>•  <a href="#">Specify 3998 Lead Kit Implant Manual</a></li> <li>•  <a href="#">Specify 2x4 Hinged Lead Kit Implant Manual</a></li> </ul>

Figure 3.4.2: AIMDs examples from Medtronic

## 4. Radio-frequency coils

This section contains the description of what an RF coil is, followed by an explanation of how it is designed and an implementation example of a High-Pass Birdcage coil.

### 4.1. Radio-frequency coil description

As it was explained in the previous section, in order to transfer energy from longitudinal magnetization to transversal magnetization and generate a detectable signal it is necessary to irradiate the patient with an RF field. This field is produced by a transmitter, responsible for pulse shape, duration power and repetition rate, and an RF coil, responsible for coupling the energy generated by the transmitter to the protons.

The RF pulse is produced by the modulation of a baseband pulse generated by a waveform generator. Once the RF pulse is created it is repeated at a user-defined repetition rate.

RF coils are one of the key components in a magnetic resonance scanner. RF coils serve for two purposes, to generate RF pulses at the precession frequency to excite the protons of the patient to be imaged (transmit coil) and to receive the signal (receive coil). The magnetic field generated by the coil,  $B_1$  field, is perpendicular to the induced  $B_0$  field. With the objective of producing high quality images the coil must satisfy two minimum requirements:

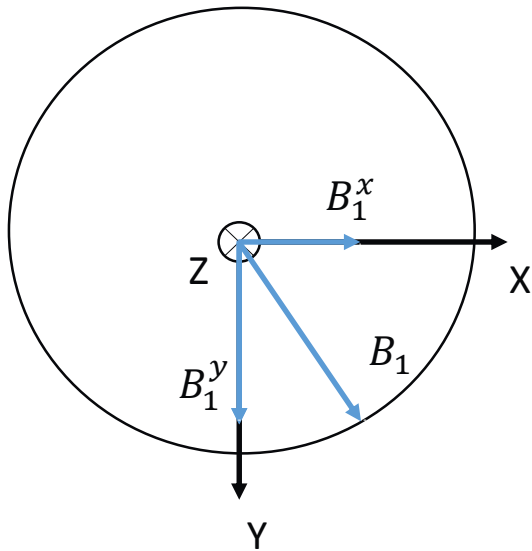
- Transmit coil: the coil must be able to generate a field as homogenous as possible inside the volume of interest. Protons need to be excited uniformly to generate clear images since the tip angle of their magnetization vector depends on the field intensity. Non-homogeneous field introduces distortion.
- Receive coil: the coil must have a high signal-to-noise ratio (SNR). In addition it must have the same reception gain at any point of the

volume. It is also recommended to fill the field of vision of the coil only with the patient/sample, thus the noise is reduced.

It is desirable to have a coil that allows quadrature excitation in reception as well as in transmission, that is to say, a circular polarization compliant coil. The main reason why is efficiency. A linearly polarized field  $B_1$  can be described as the addition of two circular components RHCP (right hand circularly polarized field) and LHCP (left hand circularly polarized field), both having amplitude of  $B_1/2$ . In the MRI scope only the component that spins in the same sense as the precession movement is utilized since it is the only one that excites the transversal magnetization. In conclusion, using circular polarization reduces the power requirement by a factor of two. Apart from increasing power efficiency, the use of circular polarization improves the SNR by a factor of  $\sqrt{2}$  since the field emitted by the transversal magnetization is circularly polarized too. If a linear probe is used the polarization mismatch loss factor is halved, as it only detects one of the linear components in which the circularly polarized field is decomposed.

In spite of the efforts made to generate a purely circular field, non-ideal conditions will always promote the apparition of non-desired components. Therefore, the RF field can be expressed as  $B_1 = B_1^+ + B_1^-$ , where  $B_1^+$  is the component that spins in line with the transversal magnetization vector and  $B_1^-$  is the one that spins in the opposite direction. The ratio between  $B_1^+$  and  $B_1^-$  offers information about the efficiency of the coil, as it relates the power spent in generating the desired field to the power wasted in the useless  $B_1^-$  component.

Circular polarization is achieved by the combination of two linear polarizations with a phase shift of 90 degrees between them. The next figure shows how circularly polarized  $B_1$  field can be decomposed in two transversal linear polarized excitations. It is considered circular polarization when the ratio (axial ratio, AR) between the two linear components is one.



$$AR = \frac{B_1^x}{B_1^y} \begin{cases} AR = 1 \text{ if circular} \\ AR = \infty \text{ or } r = 0 \text{ if linear} \end{cases}$$

Figure 4.1.1: Circular polarization axial ratio (AR)

Thanks to the branchline hybrid coupler the necessary hardware for power splitting and phase shifting can be implemented in only one device utilized for the connection of the coil to both emitter and receptor. This device introduces the 90 degrees shift for the signal to be transmitted and corrects that shift when receiving.

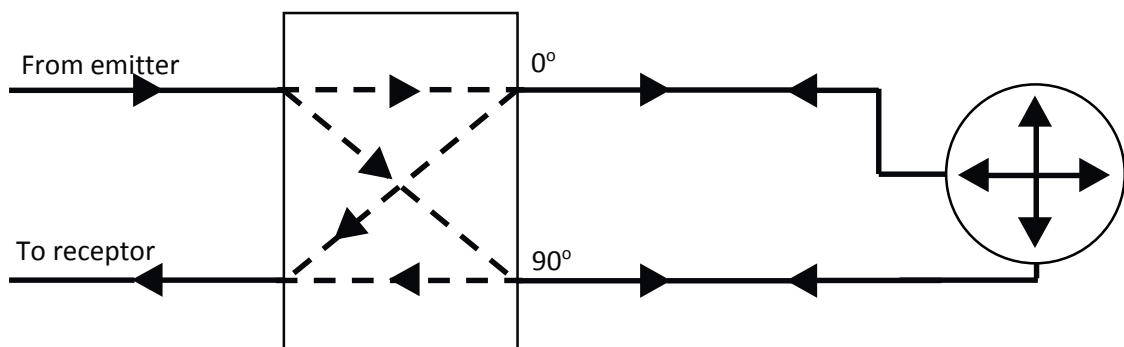


Figure 4.1.2: Branch-line hybrid connected to a coil

## 4.2. Radio-frequency coil design

Coils can be categorized into two groups, volume and surface coils. While the former provides a very homogenous field the latter has a high SNR. In the last two decades birdcage coils, which belong to the volume coils group, have become the most popular coil. This coil combines lumped capacitors with distributed inductance (legs). Capacitors make possible the storing of electrical energy without storing a field in the patient. This fact improves the efficiency of the resonator, since the flow of conduction currents in the patient is avoided [6].

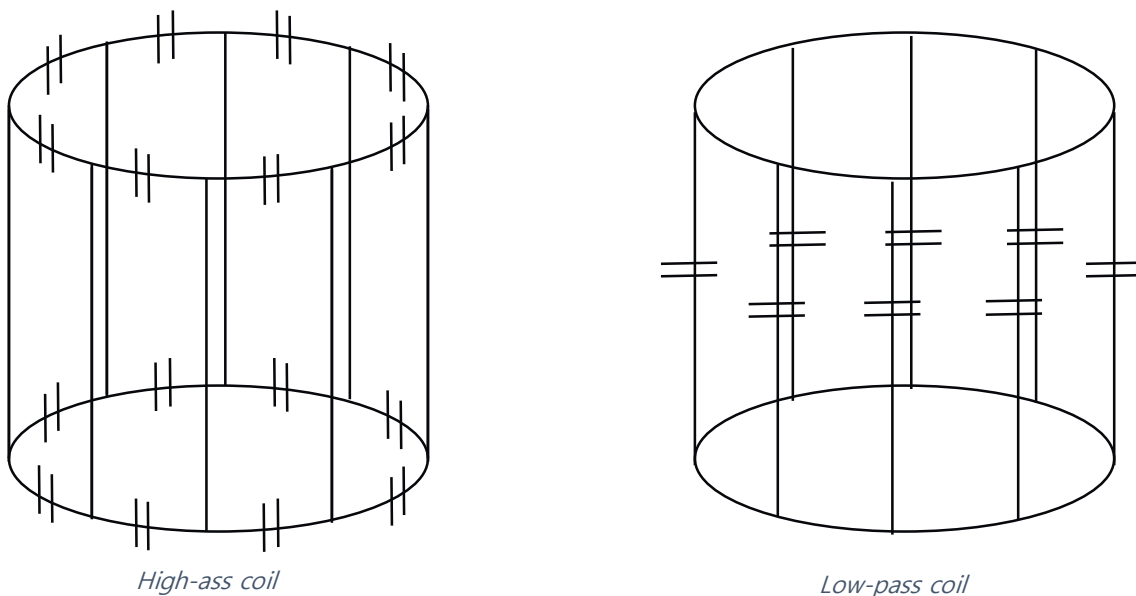


Figure 4.2.1: Birdcage coils

### 4.2.1. Concept of resonance

Although birdcage coils are usually constructed using iterative methods where capacitances are varied until the desired tuning is achieved, a more theoretical method is revisited in this final degree project.

First, it is necessary to understand the concept of resonance, consider the following RLC circuit:

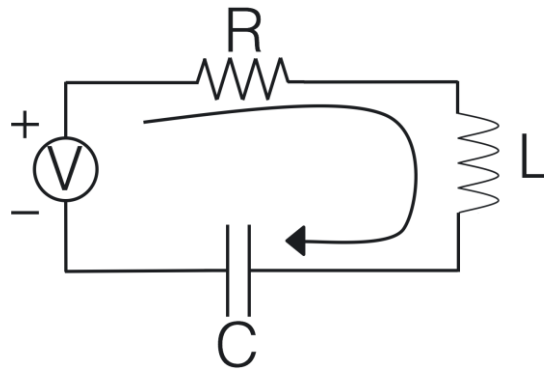


Figure 4.2.1.1: RLC circuit

By applying Kirchoff's law the next result is obtained, where  $j = \sqrt{-1}$  and  $\omega$  denotes angular frequency:

$$RI - \frac{j}{\omega C}I + j\omega L = V \quad (4.2.1.1)$$

Hence, the current is given by

$$I = V(R - \frac{j}{\omega C} + j\omega L)^{-1} \quad (4.2.1.2)$$

If  $R = 0$ , then

$$I = V(-\frac{j}{\omega C} + j\omega L)^{-1} \quad (4.2.1.3)$$

It is clear that  $I \rightarrow \infty$  when  $\omega = \omega_r = \frac{1}{\sqrt{LC}}$ .

This phenomenon is called resonance and  $\omega_r$  is known as the resonant frequency of the circuit. Of course, in a real situation, the resistance  $R$  will never be as low as 0; as a consequence the current cannot be infinity. Even so, the current would reach its maximum at that frequency. As the magnetic field produced by the current is directly proportional to the magnitude of the current, a birdcage excited at its resonant frequency can produce a magnetic field with the desired strength consuming relatively low power.

Since the resistance is not zero, some energy will be dissipated in the circuit, decreasing its quality. In order to offer a quantitative measure of the quality of the circuit, the factor  $Q$  is defined as follows:

$$Q = 2\pi \frac{\text{maximum energy stored}}{\text{maximum energy disipated per priod}} \quad (4.2.1.4)$$

For the circuit used as an example before the quality factor can be found easily,  $Q = \frac{1}{R} \sqrt{\frac{L}{C}}$ .

Frequencies  $\omega_{c1}$  and  $\omega_{c2}$ , at which the module of the frequency response drops to half of its midband value can be obtained analytically. The expression for those frequencies is:

$$\omega_{ci} = \mp \frac{R}{2L} + \sqrt{\left(\frac{R}{2L}\right)^2 + \frac{1}{\omega_r^2}} \quad i = 1,2 \quad (4.2.1.5)$$

The bandwidth is calculated as follows:

$$\Delta\omega = |\omega_{c1} - \omega_{c2}| = \frac{R}{L} \quad (4.2.1.6)$$

Combining equation (4.2.1.6) and the quality factor for a series RLC circuit we reach to the following relation between the quality factor and the bandwidth of the circuit:

$$Q = \frac{\omega_r}{\Delta\omega} \quad (4.2.1.7)$$

For complex circuits is not that easy to know the values of  $R$ ,  $L$  and  $C$  of the equivalent circuit. When this occurs (4.2.1.7) is useful for computing the quality factor.

#### 4.2.2. Equivalent circuit analysis

The typical birdcage coil structure consists of two conducting loops known as end rings (ER). End rings are connected by a number of rungs usually referred as legs, which are distributed around the perimeter of the end ring with a constant separation (shown as  $d$  in *Figure 4.2.2.1 b*). The way capacitors are distributed along the birdcage determines if the coil is low-pass (capacitors situated on legs), high-pass (capacitors placed on end rings), or band-pass (capacitors at both end rings and legs). An example of a birdcage coil is shown below in *Figure 4.2.2.1 a*, *Figure 4.2.2.1 b*) represents two consecutive legs.

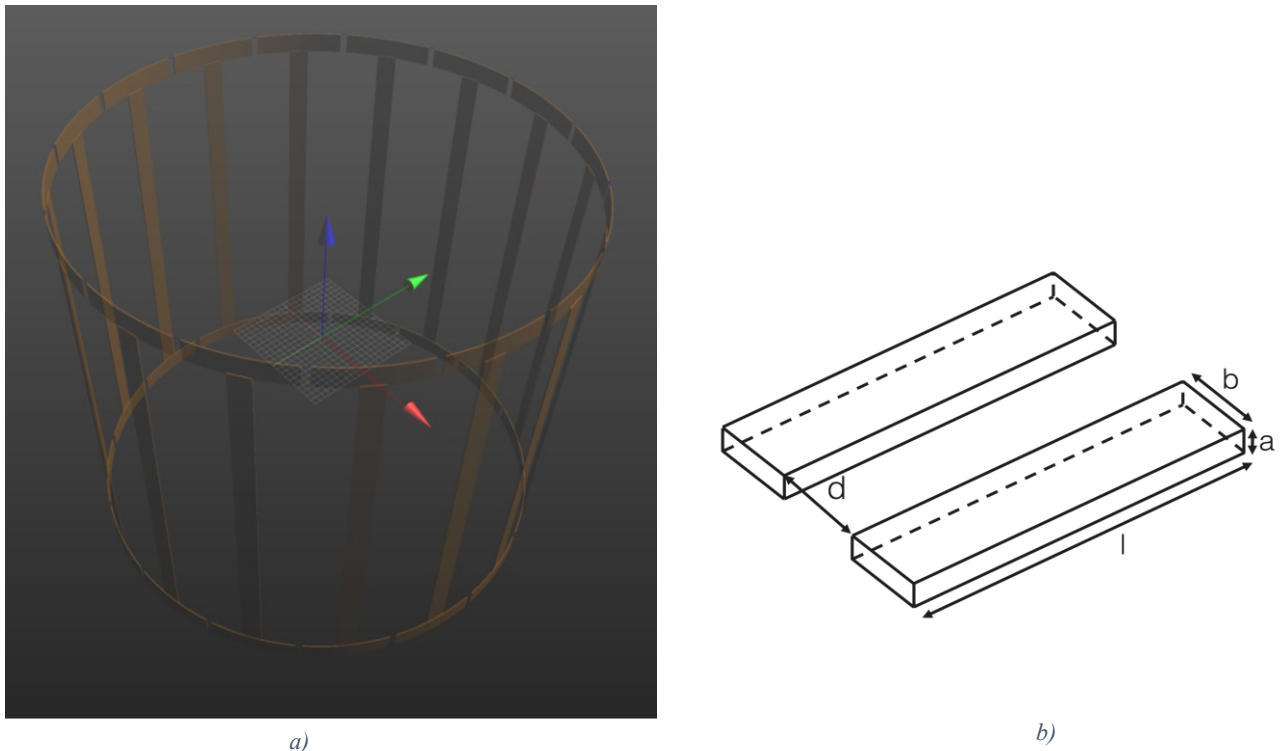


*Figure 4.2.2.1: High-pass coil model in SEMCAD X and consecutive legs representation*

With the objective of calculating the required capacitances, a circuitual equivalent of the birdcage is needed. To simplify the calculations, we will assume that parasitic resistance and inductance of the rungs are both zero. A correct calculation of the effective inductance for legs and ER is crucial when building a circuitual equivalent. The effective inductance depends on the current pattern, self-inductance and mutual inductance between conductors.

The self-inductance the rungs ( $L_n^{self}$ ) can be calculated based on the inductance calculation formula for rectangular conducting elements from [9].

$$L_n^{self} = 2l \left( \ln \frac{2l}{a+b} + 0.2235 \frac{a+b}{l} + \frac{1}{2} \right) \quad (4.2.2.1)$$

Mutual inductance ( $M_{n,m}$ ) calculation depends on the manner in which the elements are arranged. In a birdcage coil, legs are handled as parallel elements along the axis of the coil, while ER are treated as conducting segments on the transverse plane. Legs and ER mutual inductances can be obtained applying a formula for parallel and non-parallel conductors from [9].

Finally, effective inductance can be calculated using the following formula.

$$L_n = L_n^{self} + \sum_{m=1, m \neq n}^k \delta_{nm} \left| \frac{I_m}{I_n} M_{n,m} \right| \quad (4.2.2.2)$$

Function  $\delta_{nm}$  is defined by the angle  $\theta$  between the directions of the currents  $I_m$  and  $I_n$ .

$$\delta_{nm} = \begin{cases} -1, & \cos(\theta) < 0 \\ 0, & \cos(\theta) = 0 \\ 1, & \cos(\theta) > 0 \end{cases} \quad (4.2.2.2)$$

The circuit model for a band-pass birdcage coil is represented below [10].

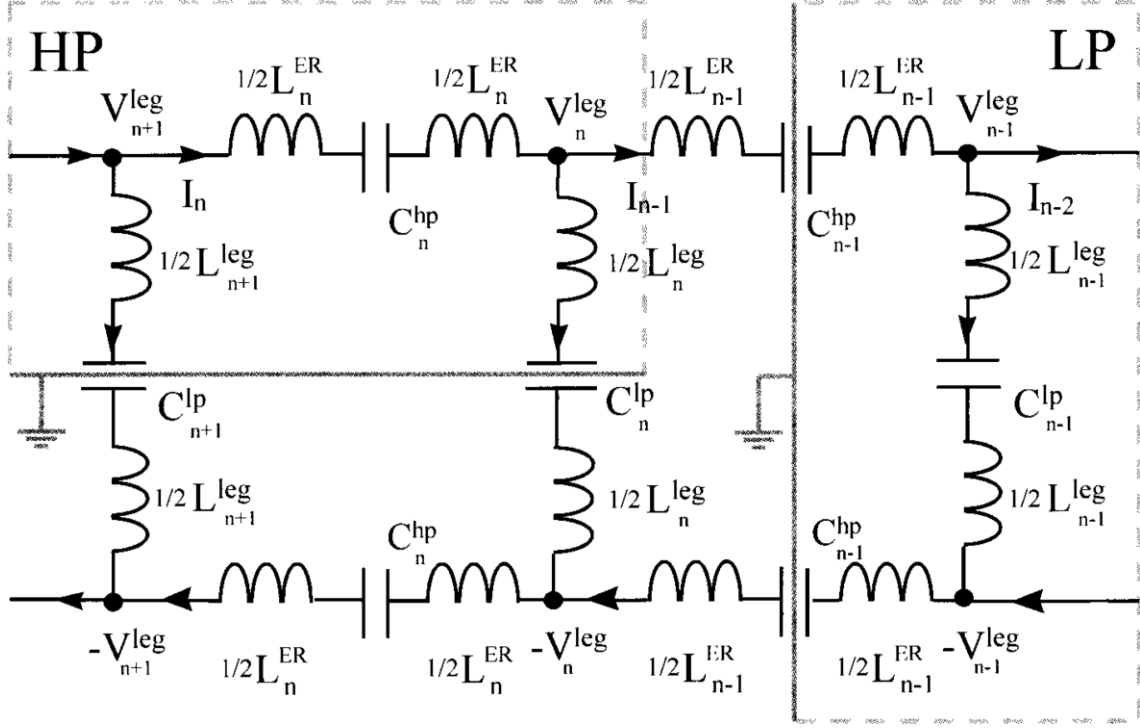


Figure 4.2.2.2: Equivalent Circuit

$L_n^{leg}$  and  $L_n^{ER}$  represent the effective inductances of the corresponding leg and ER segment, while  $C_n^{lp}$  and  $C_n^{hp}$  are the capacitances on the  $n$ th leg and ER segment. The current in each loop is designated by  $I_n$ . The voltage at the end point of the  $n$ th leg is indicated by  $V_n^{leg}$ . Both high-pass and low-pass models can be obtained from the complete band-pass equivalent.

#### 4.2.3. Calculation of ER Capacitors

In this case, the model of interest is inside the box labelled as HP (High-pass birdcage). As we assumed before, parasitic inductance and resistance are both 0, as a consequence, legs can be treated as short-circuits ( $C_n^{lp} = \infty$ ) and the virtual ground is assumed at the middle of the leg.

$$V_n^{leg} = \frac{1}{2}(I_n - I_{n-1}) [j\omega L_n^{leg} + (j\omega C_n^{lp})^{-1}] \quad (4.2.3.1)$$

$$\Delta V_n^{ER} = V_{n+1}^{leg} - V_n^{leg} = I_n [j\omega L_n^{ER} + (j\omega C_n^{hp})^{-1}] \quad (4.2.3.2)$$

$$C_n^{hp} = \left[ \frac{j\omega}{I_n} (V_{n+1}^{leg} - V_n^{leg}) + j\omega^2 L_n^{ER} \right]^{-1} \quad (4.2.3.3)$$

#### 4.2.4. Calculation of Leg Capacitors

For Low-pass birdcage (LP box) the reasoning is the same as in the previous case, but working with the ER as if they were short-circuits ( $C_n^{hp} = \infty$ ) and assuming virtual grounds at the middle of the ER segments.

$$V_{n-1}^{leg} = -\frac{1}{2}I_n \left[ j\omega L_{n-1}^{ER} + (j\omega C_{n-1}^{hp})^{-1} \right] \quad (4.2.4.1)$$

$$\Delta V_{n-1}^{leg} = V_{n-1}^{leg} - (-V_{n-1}^{leg}) = (I_{n-1} - I_{n-2})[j\omega L_{n-1}^{leg} + (j\omega C_{n-1}^{lp})^{-1}] \quad (4.2.4.2)$$

$$C_{n-1}^{lp} = \left[ \frac{j\omega}{I_{n-1} - I_{n-2}} 2V_{n-1}^{leg} + j\omega^2 L_{n-1}^{ER} \right]^{-1} \quad (4.2.4.3)$$

The only parameter that remains unknown is current. Due to cylindrical symmetry, the current  $I_n$  must satisfy the periodic condition  $I_n = I_{n+N}$ . Consequently  $N$  linearly independent solutions are found [6].

$$(I_n)_m = \begin{cases} \cos \frac{2\pi nm}{N} & m = 0, 1, 2, \dots, \frac{N}{2} \\ \sin \frac{2\pi nm}{N} & m = 1, 2, \dots, \frac{N}{2} - 1 \end{cases} \quad (4.2.4.4)$$

Where  $(I_n)_m$  represents the current in the  $j$ th loop (ER current) for the  $m$ th solution. Therefore, the current that flows through the  $n$ th leg is defined as:

$$(I_n)_m - (I_{n-1})_m = \begin{cases} -2\sin \frac{\pi m}{N} \sin \frac{2\pi m(n-0.5)}{N} & m = 0, 1, 2, \dots, \frac{N}{2} \\ 2\sin \frac{\pi m}{N} \cos \frac{2\pi m(n-0.5)}{N} & m = 1, 2, \dots, \frac{N}{2} - 1 \end{cases} \quad (4.2.4.5)$$

Examining these equations we can observe that for  $m = 0$  the value of the current is constant in the end rings and zero in the legs. On the other hand, solutions of  $m = 1$  produce current patterns similar to  $\cos \alpha$  or  $\sin \alpha$ . Knowing that uniform current patterns produce uniform magnetic fields and that sinusoidal current patterns produce uniform fields when flowing in a cylindrical

surface [6] we can conclude that both patterns are suitable for magnetic resonance applications.

### 4.3. Example of High-Pass coil construction

Before carrying out the simulation of the phantoms' behaviour when irradiated in a MRI machine is necessary to design a coil. A birdcage with the following dimensions was constructed, according with the calculations developed in (4.2.3.1 – 3) and the constraints expressed in the standard ISO10974:

- Birdcage height: 650 mm
- Birdcage radius: 375 mm
- Leg length: 560mm
- Gap between ER segments: 10 mm
- Plates thickness: 4 mm
- ER plates width: 45 mm
- Leg plates width: 25 mm

An example of a High-pass Birdcage model built in SEMCAD X was depicted in *Figure 4.2.2.1 a*.

The magnet used generated a  $B_0$  field with strength of 1.5T. Therefore, applying Larmor equation, the resonance frequency obtained was:

$$\omega_o = 1.5[T] \cdot 42.5 \left[ \frac{MHz}{T} \right] = 63.75[MHz] \approx 64[MHz]$$

Substituting the dimensions specified before in the equations defined in (4.2.2.1) and (4.2.2.2) we reach to the following values for ER and legs inductances:

$$L_{self}^{ER} = 63.22 nH; L_{eff}^{ER} = 68.70 nH$$

$$L_{self}^{leg} = 466.52 nH; L_{eff}^{leg} = 321.91nH$$

With these inductance values and the current patterns described in (4.2.4.4) and (4.2.4.5) it is possible to calculate the value of the capacitances needed to make the coil resonate at 64[MHz]:

$$C_{eff}^{hp} = 66.35 \text{ pF}$$

With the purpose of determining the effect of not taking into account the mutual inductance an approximation was made using the self-inductances instead of using effective inductances when solving the circuital model. With this approximation the value obtained was:

$$C_{self}^{hp} = 62.64 \text{ pF}$$

The result barely differs from the obtained without making approximations.

It is clear that changing the values of the capacitances will modify the frequency at which the coil resonates. If the capacitances used are  $C_{self}^{hp} = 62.64 \text{ pF}$  the frequency will be 65.87MHz instead of 64MHz. The following graph relates resonant frequency to  $C_{self}^{hp}$ .

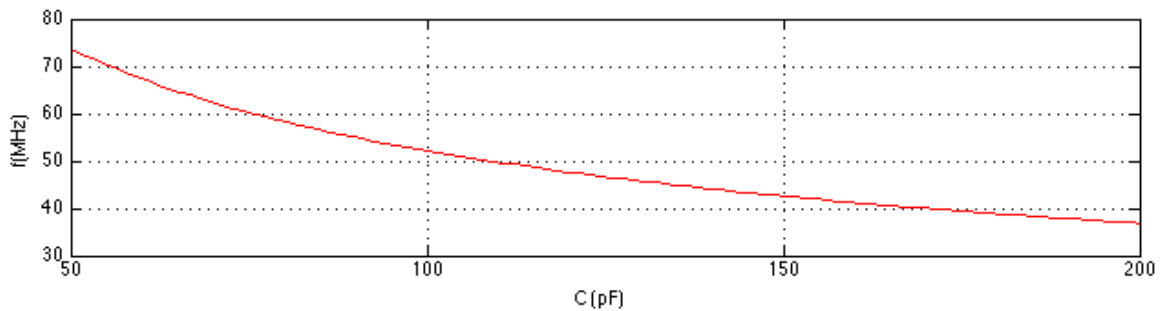


Figure 4.3.1: Dependence between resonant frequency and capacitance

It is found that  $B_1$  field variation is linearly proportional to the frequency shift produced by the use of different values of  $C_{self}^{hp}$  [6].

$$\Delta f = 100 \frac{|f - f_o|}{f_o} = 100 \frac{65.87 - 64}{64} = 2.92\%$$

$$\Delta B_1^{avg} \approx \Delta f$$

$$\Delta B_1^{max} \approx 7\Delta f = 20.45\%$$

This results show that a random capacitance variation of  $\pm 5.59\%$  is bearable as it only produces an average field variation of 2.9%. We note from the previous graphic that a decrease in  $C_{self}^{hp}$  has a bigger influence on field variation than an increase.

As it was explained previously field  $B_1$  can be separated into two components that spin in opposite directions. In the MRI scope only the component that spins in the same sense as the precession movement is studied. That component is called  $B_1^+$ , while its opposite is known as  $B_1^-$ .

$$B_1^+ = \frac{1}{2}(B(r)\hat{x} + jB(r)\hat{y}) \quad (4.3.1)$$

$$B_1^- = \frac{1}{2}(B(r)\hat{x} - jB(r)\hat{y})^* \quad (4.3.2)$$

Two empty birdcages were simulated, one with  $C_{eff}^{hp} = 66.35 \text{ pF}$  and  $f = 64 \text{ MHz}$  and other with  $C_{eff}^{hp} = 62.64 \text{ pF}$  and  $f = 65.87 \text{ MHz}$ .  $B_1^+$  field magnitude for both birdcages is plotted below. The fields were extracted from a cross-section of the centre of the coil. Results were normalized to the maximum value of each slice.

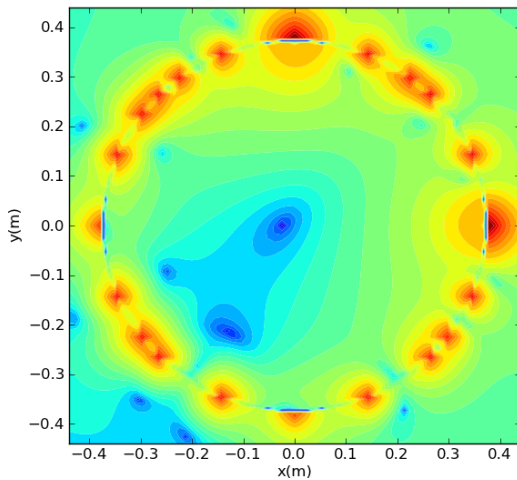


Figure 4.3.2:  $B_1^+$  for  $C=66.35 \text{ pF}$

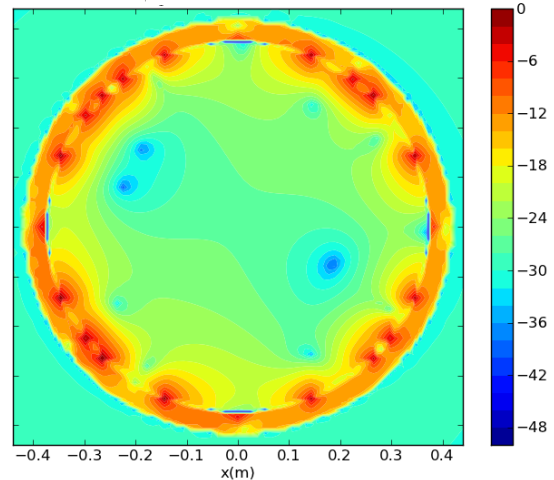
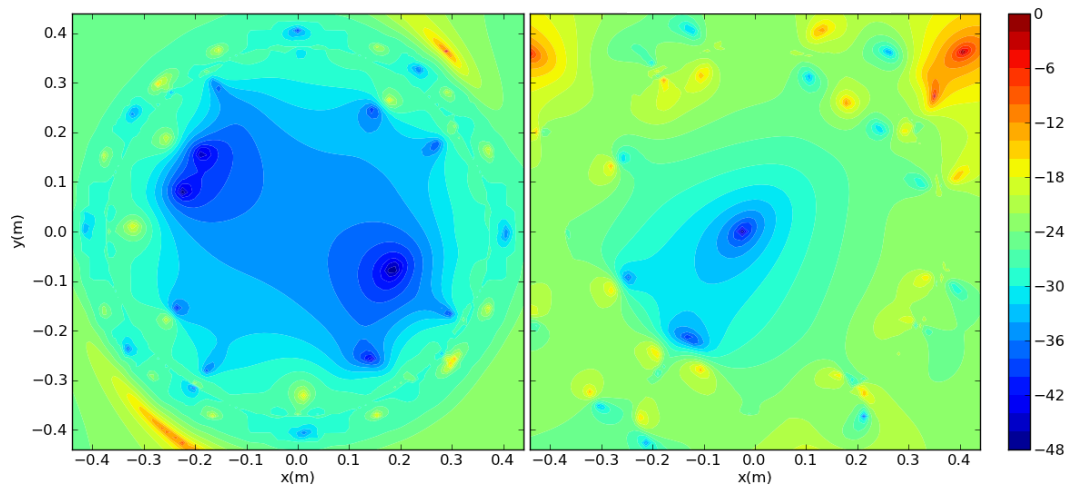


Figure 4.3.3:  $B_1^+$  for  $C=62.64 \text{ pF}$

Examining both fields, we can conclude that the field distribution is very similar for both constructions.

Another interesting parameter that should be evaluated when designing a coil is efficiency. Efficiency is determined by the ratio between  $B_1^+$  and  $B_1^-$ . That figure of merit tells how much power is successfully used in transferring energy from longitudinal magnetization to transversal compared to the power wasted. This relationship is represented in *Figure 4.3.4.* and *Figure 4.3.5.*

Predictably, the birdcage that resonates at 64MHz is considerably more efficient than the other one when both are excited in quadrature at 64 MHz.



*Figure 4.3.4:*  $B_1^+/B_1^-$  for  $C=66.35$  pF

*Figure 4.3.5:*  $B_1^+/B_1^-$  for  $C=62.64$  pF

Finally the axial ratio for  $B_1^+$  was represented. Green areas inside the red circle indicate where the axial ratio is nearly 1. This plots shows that  $B_1^+$  generated by the coil designed using approximated calculations has a purer circular polarization.

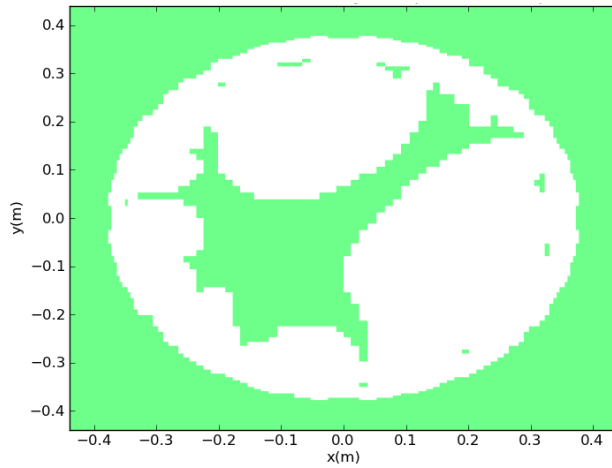


Figure 4.3.6: AR for  $C=66.35$  pF

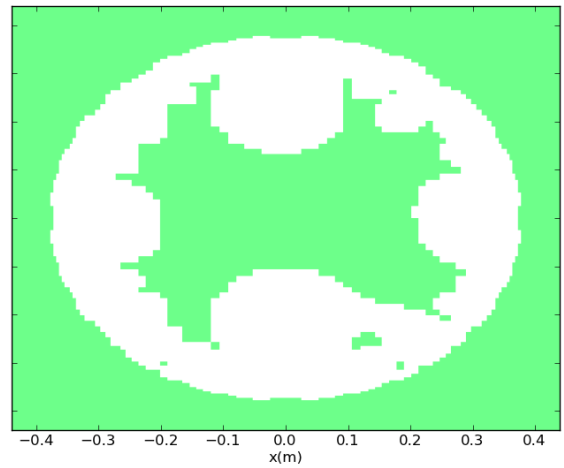


Figure 4.3.7: AR for  $C=62.64$  pF

## 5. Technical Specification ISO/TS 10974 Simulations

Although the field induced in the phantom differs on a considerable way from the fields induced in the human body, phantoms provide a good test environment that can be correlated to human situations. In this section, several pathways have been identified inside some phantoms with the goal of providing coil-phantom configurations and pathways (long enough to match actual AIMDs length) that generate a relatively uniform tangential electric field. This field must meet specifications exposed in 3.3.

For the simulations the same coil constructed in 4.3 (taking into account mutual inductances) was used. All the results are normalized to the value of  $B_1$  field in the isocentre of the empty coil.

### 5.1. Phantoms dimensions

The phantoms involved in the simulations had the following dimensions:

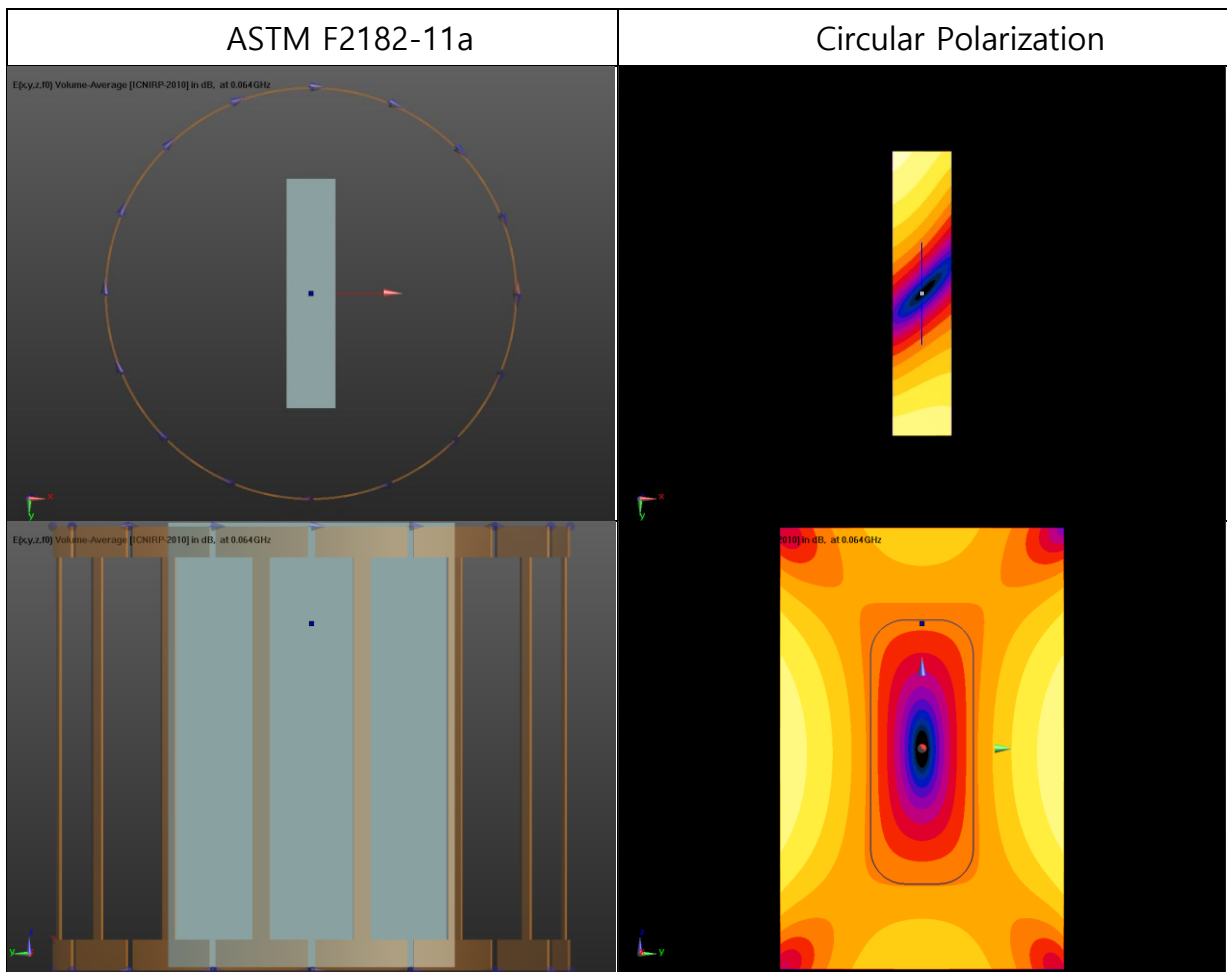
	<b>ASTM F2182- 11a [11]</b>	<b>Oval</b>	<b>Circular</b>
<b>Thickness</b>	90	90	90
<b>Height</b>	650	400	220
<b>Width</b>	420	400	220

*Table 5.1.1: Phantoms dimensions*

In practice, phantoms are filled with tissue simulating liquid. That liquid is chosen depending on the body part under study, electrical characteristics of some tissues are given in annex I. However, for the simulations, HCM and LCM configurations of 3.3 have been used.

## 5.2. High Conductivity Medium

The following result tables show the results of simulating three different phantom-coil configurations with pathways disposed with the intention of finding the most uniform tangential electric field. The phantoms used tried to emulate a high conductivity tissue using a relative electrical permittivity of 78, and a conductivity of 0.47 S/m. Analysing table I from Annex I we can consider some body parts such as bladder, brain or colon tissues as HCM.



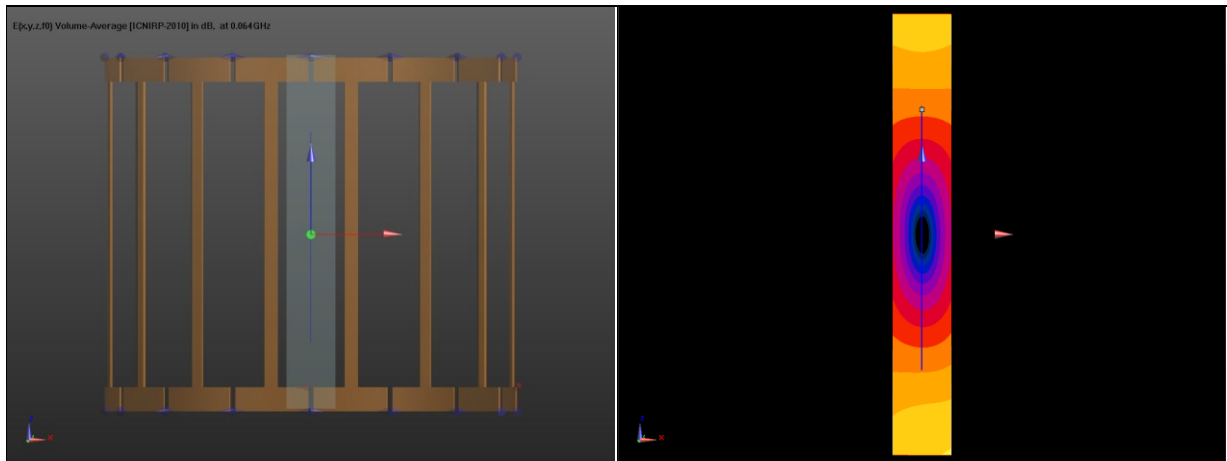


Table 5.2.1: HCM ASTM F2182-11a field plots

The following graphs show the normalized Electric field tangential to the line of the pathway. Red lines denote the  $\pm 1$ dB requirement. It is clear that this configuration meets the module specification along a considerable fraction of its length.

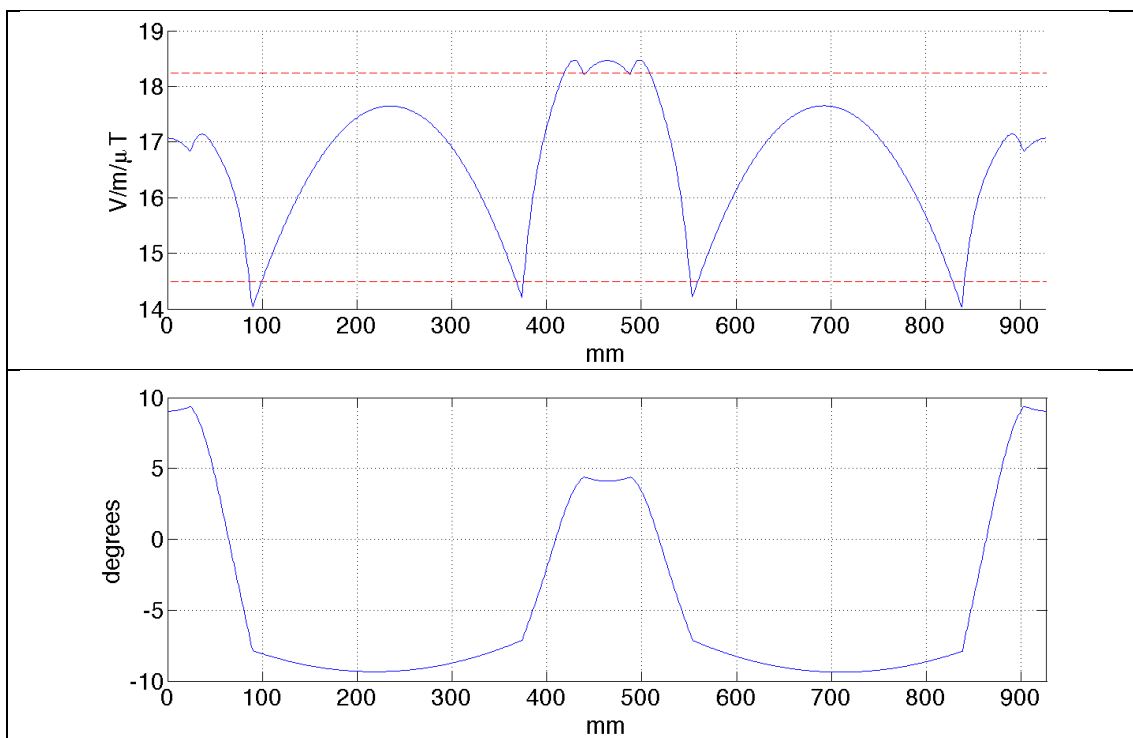


Table 5.2.2: HCM ASTM F2182-11a module and phase along the pathway

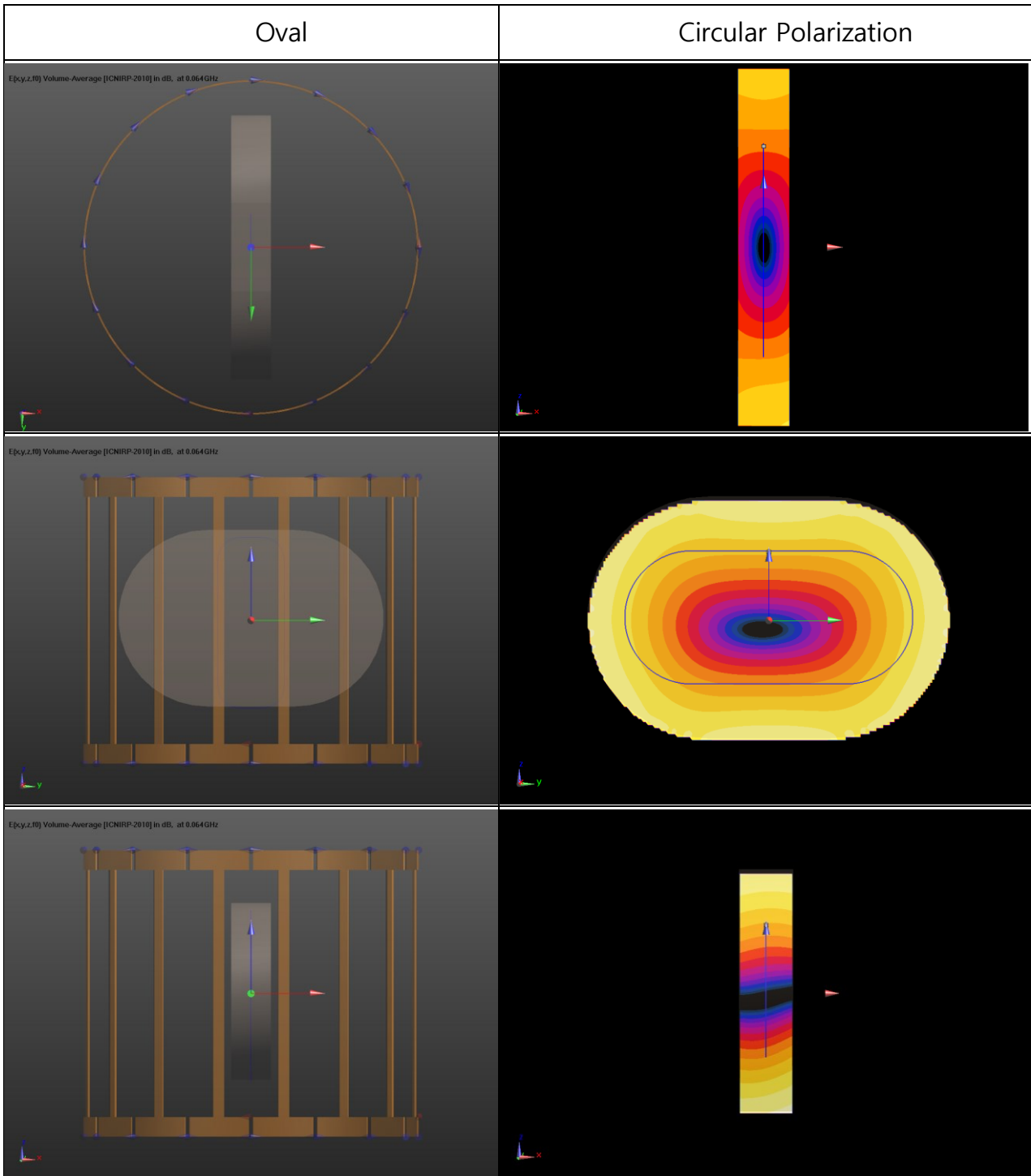


Table 5.2.3: HCM Oval phantom field plots

For the elliptical phantom and pathway configuration simulated, the tangential field specification is fulfilled all along the pathway.

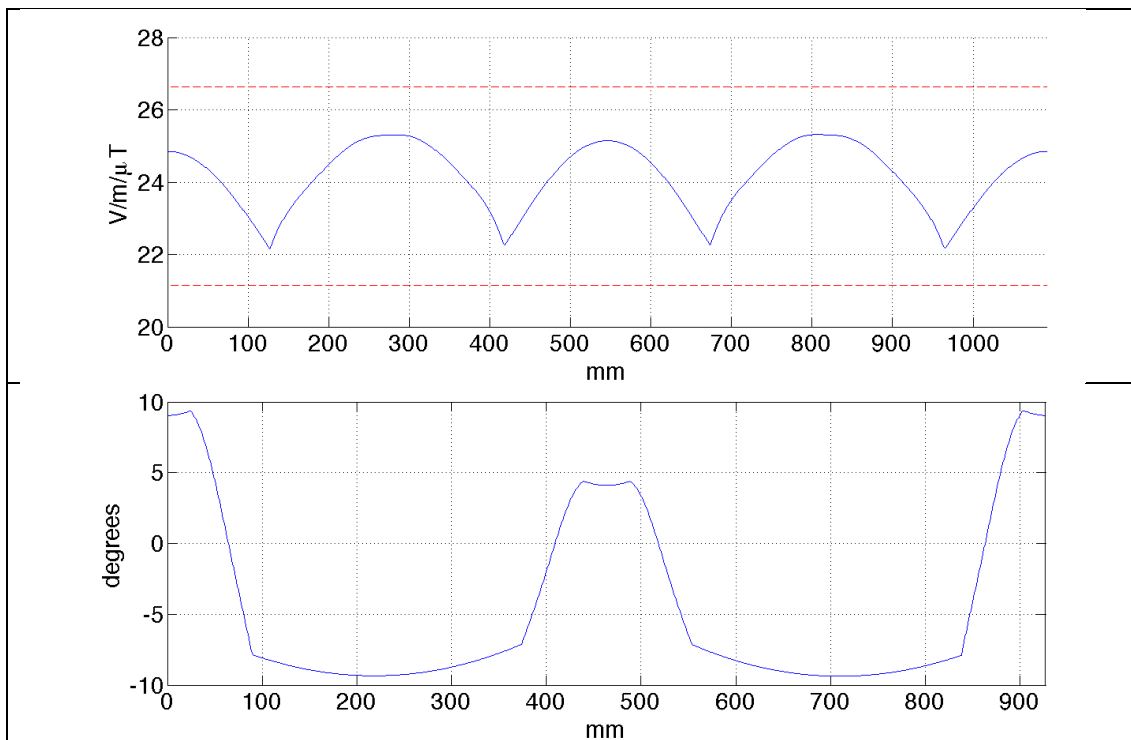


Table 5.2.4: HCM Oval phantom module and phase along the pathway

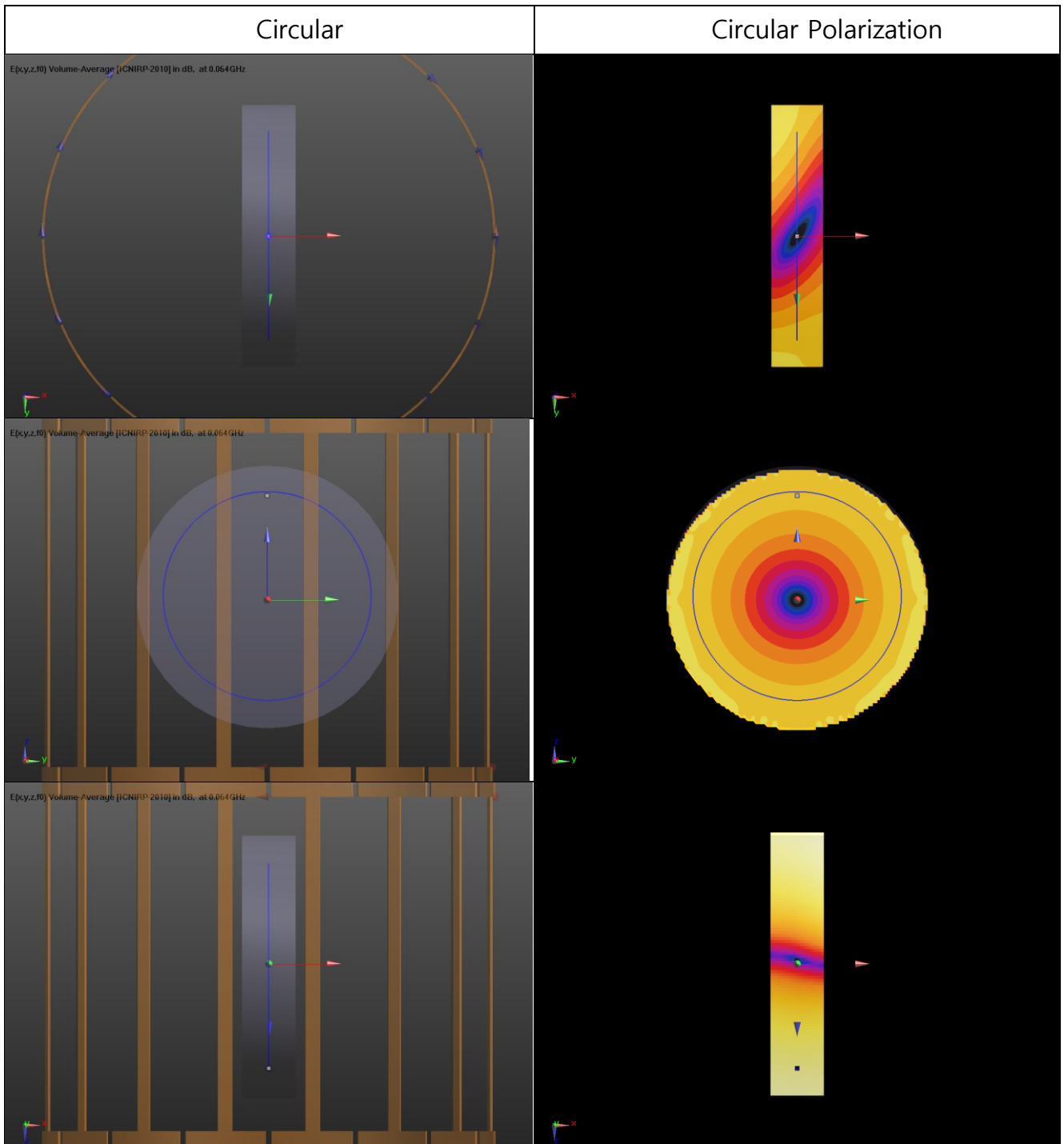


Table 5.2.5: HCM Circular phantom field plots

The requirements are also met with this circular phantom-coil configuration and the pathway depicted in the previous table.

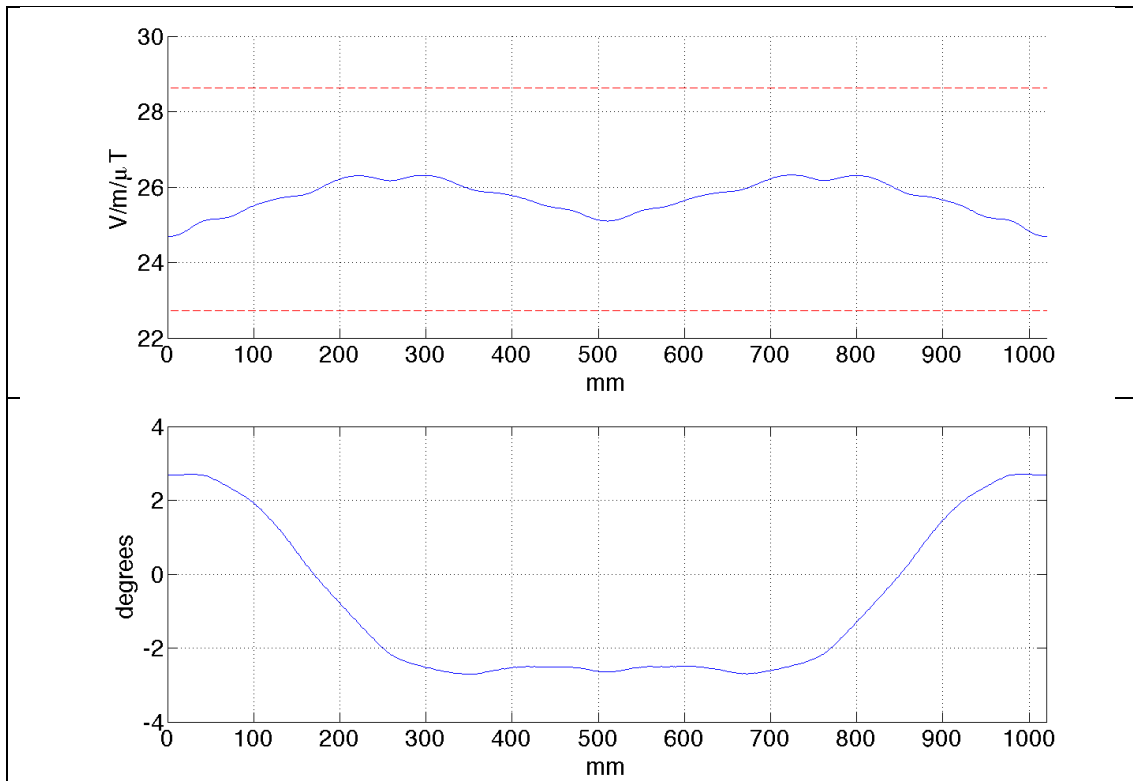


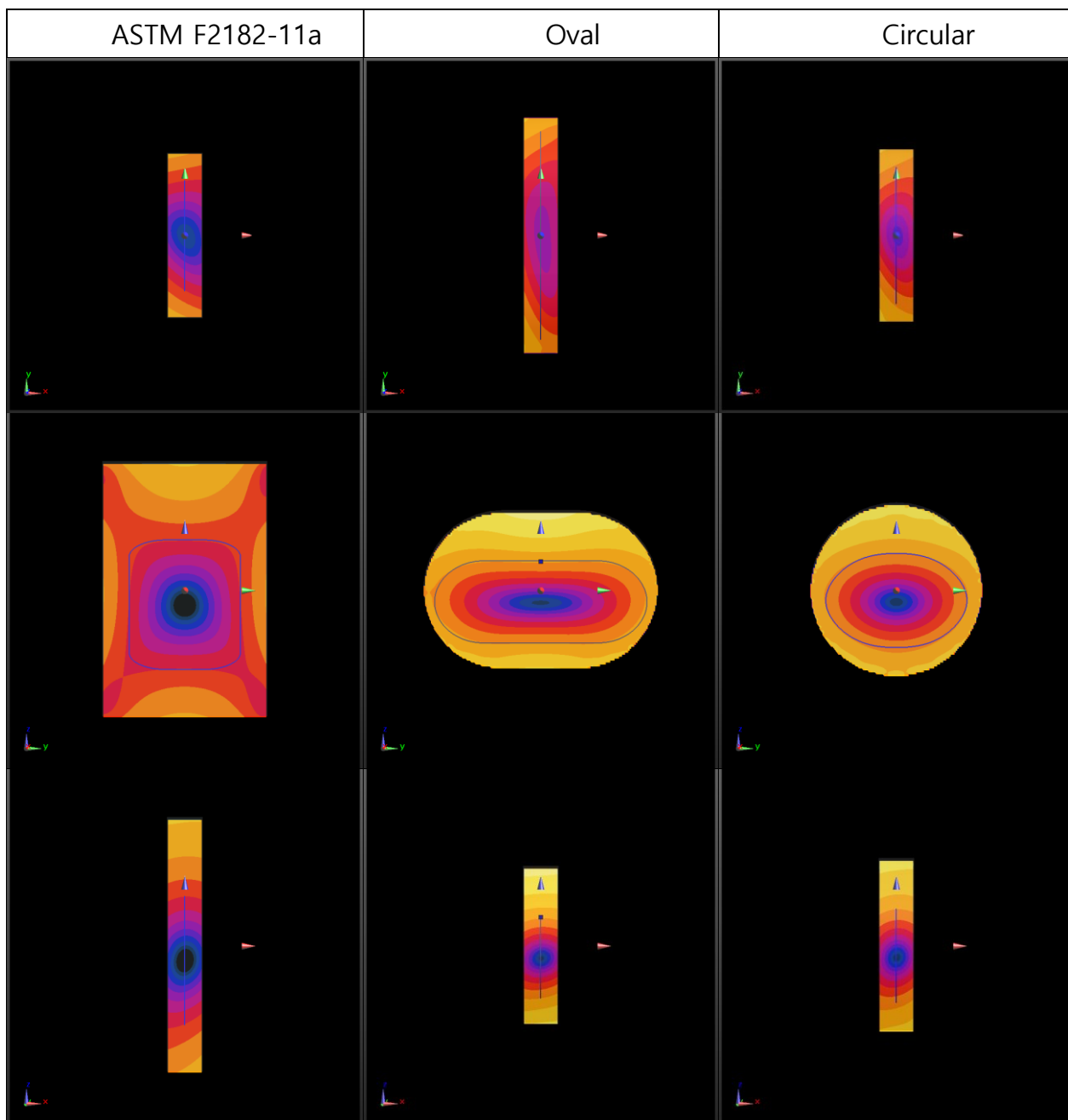
Table 5.2.6: HCM Circular phantom module and phase along the pathway

We note that for all the three HCM phantoms the phase deviation is smaller than 10 degrees.

### 5.3. Low Conductivity Medium

Changing the phantoms' EM characteristics to a relative electrical permittivity of 11.5, and a conductivity of 0.045 S/m (LCM) the following results were obtained. Observing table I once again we identify bone cortical or tooth as LCM.

Table 5.3.1: LCM phantoms field plots



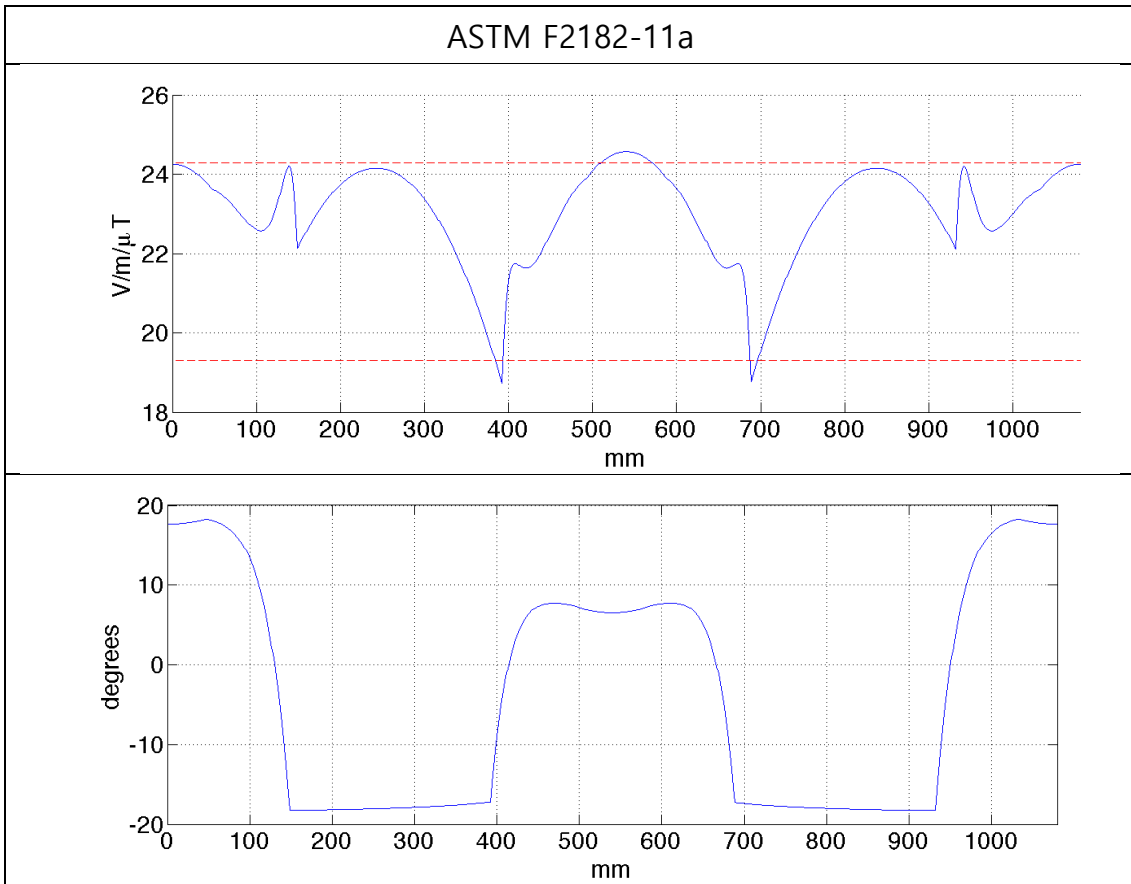


*Table 5.3.2: LCM ASTM F2182-11a module and phase along the pathway*

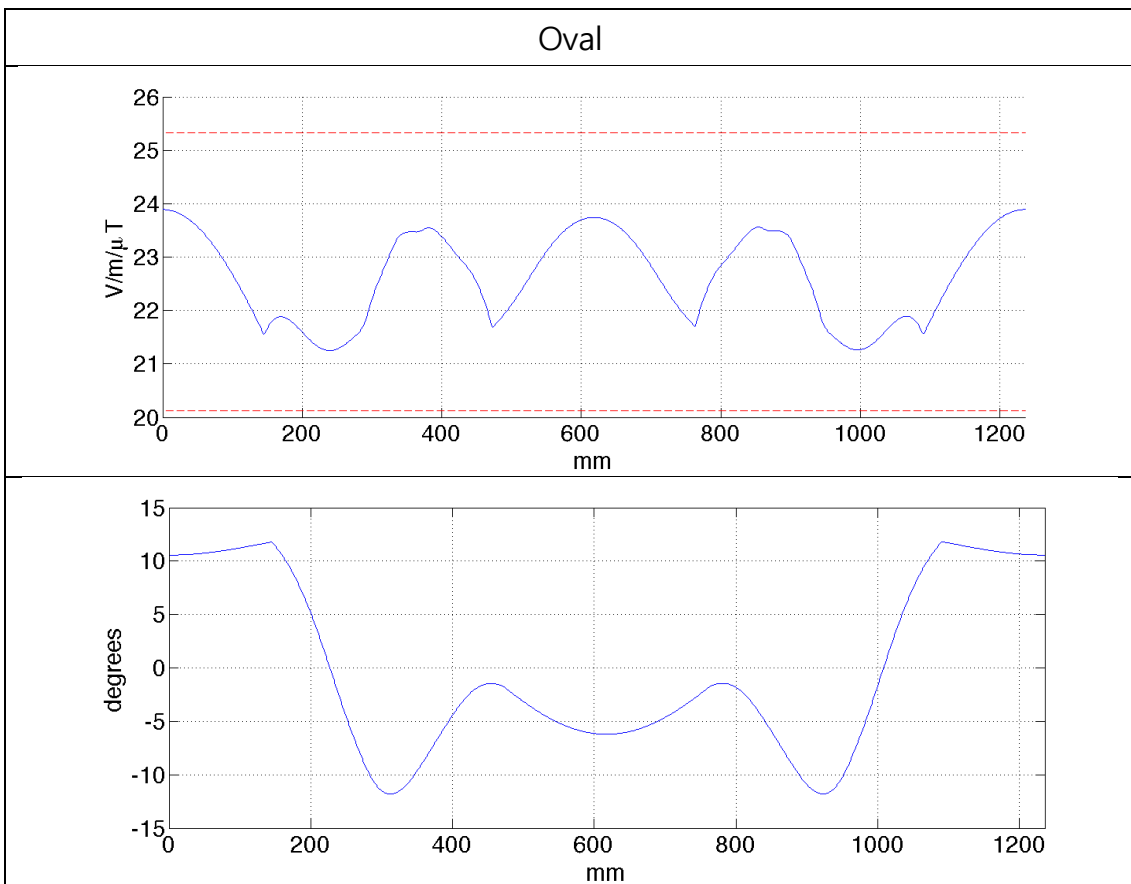


Table 5.3.3: LCM Oval phantom module and phase along the pathway

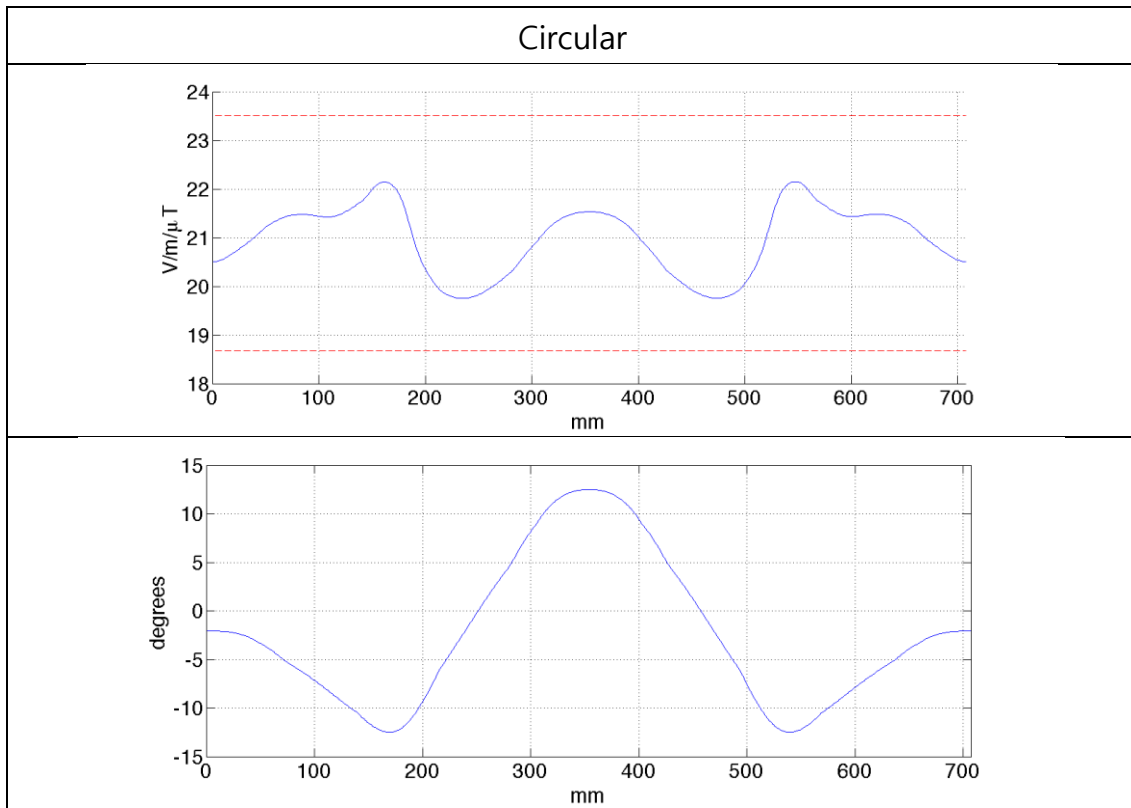


Table 5.3.4: LCM Circular phantom module and phase along the pathway

In spite of the phase deviation increase that takes place when simulating LCM phantoms, the implants still meet the specification of maximum deviation of  $\pm 20$  degrees.

## 6. Conclusions

### 6.1. Conclusions

In this work, we have studied the basics of MRI and have acquired some notions about MRI safety and SAR. Moreover we studied the functions and design process of one of the key elements of an MRI scanner, the RF coil.

During the design of the RF coil we tried to calculate the capacitances needed to make the birdcage coil resonate at the desired frequency without taking into account the mutual inductance of the plates that form the coil with the purpose of simplifying the process. We observe that although the capacitances obtained by applying the approximation offered a similar field distribution and purer circular polarization, compared to the exactly calculated coil, the decrease in the efficiency of the coil makes the estimation not worthwhile.

Once the basic concepts were interiorized, we proceeded with the construction of three phantom-coil configurations specifically disposed with the intention of finding a pathway that constitutes an isoelectric line. Each configuration was later duplicated, having one with a high conductivity phantom and another one with a low conductivity phantom. The results show that for longer implant test the isoelectric condition is not always matched, it is easier to achieve it along a shorter straight line. Furthermore, we observe that in the low conductivity model the phase deviation obtained is significantly higher. We note that the field distribution varies notably from one phantom to another when using the same coil. Although it seems that the shape of the phantoms is a determining factor, we cannot state that the use of a certain phantom offers more accurate results than the use of another model. It would be more effective to use layered phantoms that emulate the discontinuities inside the human body rather than designing a human-shaped model.

## 6.2. Future Work

In order to accomplish a full analysis of the phantom-coil configuration simulated in the previous chapter and validate the implant it would be necessary to carry out a study of the temperature increase that would take place in the surrounding tissues when a metallic implant is placed along the pathway. Moreover, it is also necessary to validate the test setup. This validation, explained in the Annex I of the standard [1], should be repeated at least once per year or whenever there are setup or instrumentation changes, etc. For the validation of the setup, it is necessary to use one of the two highly characterized implants provided by the standard. For both validations, thermal simulations are launched after electromagnetic simulations are done.

## 7. References

- [1] Assessment of the safety of magnetic resonance imaging for patients with an active implantable medical device. ISO/TS 10974. 2012
  
- [2] ISO/TS 10974. 2015, currently on revision
  
- [3] Hans H. Schild: MRI made easy, Schering, Berlin, 1990
  
- [4] Dominik Weishaupt, Victor D. Köchli, and Borut Marincek: How does MRI work? , Springer, Berlin, 2006
  
- [5] Catherine Westbrook and Carolyn Kaut: MRI in practice, Blackwell Publishing, Oxford, 2000
  
- [6] Jianming Jin: Electromagnetic Analysis and Design in Magnetic Resonance Imaging, CRC Press, Boca Raton, USA, 1999
  
- [7] Alan W. Preece: Safety Aspects of Radio Frequency Effects in Humans from Communication Devices, CRC Press, Bristol, 2002
  
- [8] Semcad X Reference Manual, Speag, Zurich. 2013
  
- [9] Grover, FW: Inductance calculation, Van Nostrand, New York, 1946
  
- [10] Chih-Liang Chin, Christopher M. Collins, Shizhe Li, Bernard J. Dardzinski, and Michael B. Smith, Birdcagebuilder: Design of Specified-Geometry Birdcage Coils with Desired Current Pattern and Resonant Frequency, National Institute of Health, 2002
  
- [11] Standard Test Method for Measurement of Radio Frequency Induced Heating On or Near Passive Implants during Magnetic Resonance Imaging American Society for Testing Materials (ASTM) F2182



## ANNEX I: Dielectric parameters

	64 MHz		128 MHz	
	$\epsilon_r$	$\sigma$ in S/m	$\epsilon_r$	$\sigma$ in S/m
Bladder	68,6	0,29	21,9	0,30
Blood	86,4	1,21	73,2	1,25
Bone cortical	16,7	0,06	14,7	0,07
Brain grey matter	97,4	0,51	73,5	0,59
Brain white matter	67,8	0,29	52,5	0,34
Cartilage	62,9	0,45	52,9	0,49
Cerebellum	116,4	0,72	79,7	0,83
Cerebrospinal fluid	97,3	2,07	84,0	2,14
Colon	94,7	0,64	76,6	0,71
Cornea	87,4	1,00	71,5	1,06
Eye Sclera	75,3	0,88	65,0	0,92
Fat	6,5	0,035	5,9	0,037
Gall bladder	105,4	1,48	88,9	1,58
Heart	106,5	0,68	84,3	0,77
Kidney	118,6	0,74	89,6	0,85
Lens	60,5	0,59	53,1	0,61
Liver	80,6	0,45	64,3	0,51
Lung	75,3	0,53	63,7	0,58
Mucous membrane	76,7	0,49	61,6	0,54
Muscle	72,2	0,69	63,5	0,72
Nerve	55,1	0,31	44,1	0,35
Oesophagus	85,8	0,88	74,9	0,91
Ovary	106,8	0,69	79,2	0,79
Pancreas	73,9	0,78	66,8	0,80
Prostate	84,5	0,88	72,1	0,93
Skin dry	92,2	0,44	65,4	0,52
Small intestine	118,4	1,59	88,0	1,69
Spinal chord	55,1	0,31	44,1	0,35
Spleen	110,6	0,74	82,9	0,84
Stomach	85,8	0,88	74,9	0,91
Tendon	59,5	0,47	51,9	0,50
Testis	84,5	0,88	72,1	0,93
Thymus	73,9	0,78	66,8	0,80
Tongue	75,3	0,65	65,0	0,69
Tooth	16,7	0,06	14,7	0,07

Uterus	92,1	0,91	75,4	0,96
Vitreous humour	69,1	1,50	69,1	1,51

*Table I: Dielectric parameters of body tissue*

## ANNEX II: Worst-case phase weighting factors for a single conductive lead

Length as function of electrical resonant length	Worst-case phase weighting factor
0,2	1,0
0,4	1,0
0,6	1,0
0,8	1,0
1,0	1,0
1,2	1,1
1,4	1,2
1,6	1,3
1,8	1,4
2,0	1,5
2,2	1,6
2,4	1,7
2,6	1,8
2,8	1,9
3,0	2,0

*Table II: Worst-case phase weighting factors for a single conductive lead (not including helical structures and structures with lumped elements)*